Steel and Composite Structures, *Vol. 33, No. 2* (*2019*) *261-275*
DOI: https://doi.org/10.12989/scs.2019.33.2.261

On axial buckling and post-buckling of geometrically imperfect single-layer graphene sheets

Yang Gao [1a], Wan-shen Xiao*[1] and Haiping Zhu [2a]

[1] *State Key Laboratory of Advanced Design and Manufacturing for Vehicle Body*, *Hunan University*, *Changsha*, *410082*, *China*
[2] *School of Computing*, *Engineering and Mathematics*, *Western Sydney University*, *Locked*, *Bag 1797*, *Penrith*, *NSW 2751*, *Australia*

(*Received May 11, 2019, Revised September 27, 2019, Accepted October 1, 2019*)

Abstract. The main objective of this paper is to study the axial buckling and post-buckling of geometrically imperfect single-layer graphene sheets (GSs) under in-plane loading in the theoretical framework of the nonlocal strain gradient theory. To begin with, a graphene sheet is modeled by a two-dimensional plate subjected to simply supported ends, and supposed to have a small initial curvature. Then according to the Hamilton's principle, the nonlinear governing equations are derived with the aid of the classical plate theory and the von-karman nonlinearity theory. Subsequently, for providing a more accurate physical assessment with respect to the influence of respective parameters on the mechanical performances, the approximate analytical solutions are acquired via using a two-step perturbation method. Finally, the authors perform a detailed parametric study based on the solutions, including geometric imperfection, nonlocal parameters, strain gradient parameters and wave mode numbers, and then reaching a significant conclusion that both the size-dependent effect and a geometrical imperfection can't be ignored in analyzing GSs.

Keywords: geometric imperfection; perturbation method; graphene sheets; nonlocal strain gradient theory

1. Introduction

In this decade, various allotropes of carbon, ranging from fullerenes (0D), to carbon nanotubes (1D), and to graphene (2D), have captured tremendous attentions within the related research communities due to their lots of special and superior properties (Hussein and Kim 2018, Singh and Patel 2018, Wang *et al*. 2018, Christy *et al*. 2018, Hosseini *et al*. 2017). Among those emerging carbon-based solid materials, graphene, a two-dimensional and only one single atomic layer of carbon, can offer not only the potential applications in each industry but also more importantly the next generation graphene-based devices for nanoelectro-mechanical systems (NEMS) and energy storage (Yan and Lai 2018, Zhang *et al*. 2018, Wu *et al*. 2018, Kiani 2017, Sadeghirad *et al*. 2015, Soleimani *et al*. 2019, Tahouneh *et al*. 2018, Hosseini and Zhang 2018, Kumar and Srivastava 2016). Since graphene being isolated by Novoselov *et al*. (2004), the extraordinary performances of the material were reported that the elastic modulus, ntrinsic tensile strength, thermal conductivity and surface-to-mass ratio are 1 TPa, 130 GPa, 4840–5300 W/(mK) and 2600 m^2/g, the results of which are significantly higher than those of composites (Yang *et al*. 2018a). Consequently, the study of monolayer graphene sheet and its derivative has been elevated from a fringe topic to a central analytic concern in recent years

The discovery of mechanical behaviors of graphene sheets was, is and will be a hot topic for researchers. Pradhan and Murmu (2009) investigated the small scale effect on the critical buckling of single layer graphene sheets in the theoretical framework of the nonlocal elasticity theory. Afterwards, the study of shear buckling of single layer graphene sheets was performed by Shahsavari *et al*. (2017), who utilized different non-classical theories, such as sinusoidal shear deformation theory, polynomial shear deformation theory, exponential shear deformation theory and hyperbolic shear deformation theory, to reveal the difference between the size-dependent shear buckling loads predicted by various nonlocal strain gradient theories. Yang *et al*. (2016) and Shen *et al*. (2017) respectively analyzed the buckling and post-buckling of functionally graded multilayer graphene sheets not subjected to electric potential and subjected to electric potential. Except these static analyses of nanostructures made of graphene sheets, Ebrahimi and Barati (2018a) for the first time undertook the analysis of damping vibration of graphene sheets featuring uniform hygro-thermal distribution, the results of which state that the hygro-thermal loading not only increases the stiffness of plate but also arguments the natural frequencies aligned with the critical damping coefficient. With the aid of contionuum mechanical theories, researchers provided analytical solutions of linear and nonlinear vibration for the discoveries of bilayer graphene thin films (Yang *et al*. 2018b, Ebrahimi and Barati 2018b, Zhan *et al*. 2018), and for the exploration of multiple graphene sheets embedded in an elastic medium (Wu and Chen 2018, Cong and Duc 2018, Guo *et al*. 2018). Also, Allahyari and Kiani (2018) developed a conventional analytical approach to study vibration of an annular graphene sheet, the purpose of which is to further examine the defective size-dependent effect on the response of annular graphene sheets. Differing

*Corresponding author, Professor,
E-mail: xwshndc@126.com

ISSN: 1229-9367 (Print), 1598-6233 (Online)

from the aforementioned studies, Korobeynikov *et al*. (2018) attempted to acquire the accurate adjustment of the geometric and material parameters of beam elements, and then using them to model interactions between carbon atoms of single-layer graphene sheets.

Although many scholars have achieved considerable achievements for structural analysis of perfect components made of graphene sheets through employing those reasonable continuum mechanical theories, the literature on the topic of geometrically imperfect graphene sheets is not enough. However, the phenomenon that the graphene is not a perfect flat sheet exposed to any nonzero temperature has been not only indeed observed at the experimental analyses, but also successfully simulated by means of molecular simulations (Meyer *et al*. 2007, Fasolino *et al*. 2007, Bao *et al*. 2009). To date, there is a few researches relevant to the mechanical response of nonflat graphene sheets in the open literature. For instance, Wang *et al*. (2017) adopted the first-principle density functional theory to cast light on the thermal and optical properties of actual imperfect graphene, where the physical properties of graphene phonon were determined via the density functional perturbation theory, and then the results showed that the perfect graphene can be shifted into the imperfect graphene with the peaks of phonon density improving from 40 and 45.5 THz to 40.5 and 46 THz. Similarly, the team led by Yengejeh *et al*. (2017) used the density functional theory combined with the finite element method to elevate the vicinity of the influence of defects, whose the crucial findings presented that the fundamental frequency of imperfect graphene sheets continues to decline in that occuring microsopic imperfections to the formulation of nanomaterials. The study for the vibration of the microsystem consisted of three-layered geometrically imperfect sheardeformable sheets was undertaken by Ghayesh *et al*. (2017), who concluded that both the stiffness-hardening effect and the stiffness-softening effect are present at the same time for relatively larger initial imperfections, but the stiffness-softening effect is reduced for relatively smaller initial imperfections. For the effect of different porosity distributions on functionally graded graphene sheets, Barati and Zenkour (2018a) explored that the influence of uniform, symmetric and asymmetric porosity distributions on the response of vibration frequencies. Additionally, Ghavanloo (2017) firstly tackled the problem, the stability of geometrically imperfect circular graphene sheets with a radial load, the major contribution of which was to show the axisymmetric deformation of geometrically imperfect circular graphene sheets subjected to a uniform load. More works can be found in references (Barati and Zenkour 2017a, b, 2018b, c, d, 2019, Mirjavadi *et al*. 2018a)

Owing to the size of graphene sheets being on the nanometer scale, the size-dependent effect on the mechanical behaviors of nanostructures has been becoming more noteworthy (Ghayesh 2018b, 2018c, 2019a, b, c, d, e, f, g, Ghayesh and Farokhi 2015, Ghayesh *et al*. 2013b, 2015, 2016). It is not uncommon to utilize experimental methods, molecular dynamic simulations as well as continuum mechanical theories to perform the study of the size-dependent effect on nanostructures. Nevertheless, theoretical analyses based on various continuum mechanical theories are growing in importance, because of consuming much time encountered in each molecular dynamic simulations and unsatisfying the specific laboratory requirements, such as environment and boundary conditions etc, in each experimental test. At present, since the nonlocal strain gradient theory as a higher-order non-classical theory being proposed by Lim *et al*. (2015), the theory simultaneously accounting for both the effect of stiffness-hardening and the effect of stiffness-softening has been widely applied into the nanostructural analyses (Lu *et al*. 2017a, b, Li *et al*. 2018, Faleh *et al*. 2018, Ghayesh 2018a, Barretta and Sciarra 2018, Karami *et al*. 2018, Apuzzo *et al*. 2018, Zhu and Li 2017, Shahsavari *et al*. 2018, Shafiei and She 2018, Xu *et al*. 2017, Malikan *et al*. 2018, Malikan and Nguyen 2018, Zenkour and Abouelregal 2015, Belkorissat *et al*. 2015, Ebrahimi *et al*. 2016, Ebrahimi and Barati 2016, 2017, Barati 2017, Mirjavadi *et al*. 2018b, 2019). Nevertheless, the above-mentioned studies all ignore the defect of nanostructures, resulting in some inevitable errors in the prediction of mechanical behaviors of nanostructures. To the authors' knowledge, up to now, only two studies involving the influence of geometrical imperfection on the mechanical response of nanostructures have been carried out in the theoretical framework of the nonlocal strain gradient theory. One is the research conducted by Liu *et al*. (2018), who explored nonlinear vibration of geometrically imperfect nanobeams made of functionally graded materials, the other is the research conducted by Nematollahi and Mohammadi (2019), who investigated nonlinear vibration of geometrically imperfect sandwich nanoplates. Thus, it is worth performing such research to analyze the effects of the nonlocal parameters and the material characteristic parameters on axial buckling and post-buckling of geometrically imperfect nanoplates.

In order to obtain the analytical solution from the nonlinear governing equations, we in this paper introduce a two-step perturbation method that was put forward by Shen and Zhang (1988) in the analysis of post-buckling of isotropic plates. Compared with the traditional perturbation method, this method can provide a perfect physical assessment with respect to the influence of respective parameters on the analytical solutions, since it is unnecessary to derive the forms of each-order solution that is capable of acquiring step by step (Shen 2013). To date, the method has been extensively applied into the nonlinear analyses of structures. She and his colleagues employed the two-step perturbation method in conjunction with a general higher order refined beam model to study thermal post-buckling of functionally graded tubes (She *et al*. 2017a, b), nonlinear bending of functionally graded shells (She *et al*. 2019) and curved tubes with even porosity distribution (She *et al*. 2019) and thermal buckling of functionally graded beams considering the physical neutral surface (She *et al*. 2017d), in which the displacement and angle of the components were set as perturbation parameters, and then acquiring the approximate analytical solutions that include the maximum dimensionless flexural deflection to the second power. Even if the researchers also conducted the same approach to obtain the approximate analytical

solutions in these papers (Sahmani *et al*. 2015, 2016, Sahmani and Aghdam 2017a, b, Shen 2007, Shen *et al*. 2018), the displacement and the airy stress function were set as perturbation parameters in the course of acquiring a series of perturbation equations, the solutions of which include the maximum dimensionless flexural deflection to the forth power. Differing from the precious works, the authors in this work derive the post-buckling of analytical solutions, containing the maximum dimensionless flexural deflection to the sixth power, and then making a comparison with that to the forth power.

As outlined in the preceding part, there is no researcher to investigate axial buckling and post-buckling of geometrically imperfect nanoplates or single-layer graphene sheets in the theoretical framework of the nonlocal strain gradient theory. Thus, the present study is motivated by this reason. The authors in this paper are first to present a new nonlinear size-dependent geometrically imperfect plate model via using the nonlocal strain gradient theory. Then, by employing the Hamilton's principle, the nonlinear governing equations of nanoplates are derived on the basis of the classical-plate theory. Subsequently, the approximate analytical solutions that includes the maximum dimensionless flexural deflection to the sixth power for the first time are obtained through using a two-step perturbation method. Finally, a detailed parametric study is carried out based on the analytical solutions, including geometric imperfection, nonlocal parameters, strain gradient parameters and wave mode numbers.

2. Preliminaries

Fig. 1 illustrates a schematic model of single-layer graphene sheet (GS) with thickness h, width b and length a under uniform uniaxial in-plane compression. The origin of coordinate system (X, Y, Z) is set at the corn of nanoplate, and X, Y and Z axes are respectively along the directions of length, width and thickness.

Based on the classical plate theory, the displacement field (u_x, u_y, u_z) of a single-layer graphene sheet can be expressed as (Farokhi and Ghayesh 2015)

$$\begin{aligned} u_x &= u(x,y) - z\frac{\partial w(x,y)}{\partial x} \\ u_y &= v(x,y) - z\frac{\partial w(x,y)}{\partial y} \\ u_z &= w(x,y) + w^*(x,y) \end{aligned} \tag{1}$$

where $u(x,y)$, $v(x,y)$, $w(x,y)$ and $w^*(x,y)$ respectively stand for the displacement components of the middle surface of GSs and the initial geometric imperfection in the out-of-plane direction. Subsequently, in accordance with von karman geometrical nonlinear theory, the respective strain components are written as

$$\begin{Bmatrix} \varepsilon_{xx} \\ \varepsilon_{yy} \\ \gamma_{xy} \end{Bmatrix} = \begin{Bmatrix} \dfrac{\partial u_x}{\partial x} + \dfrac{1}{2}\left(\dfrac{\partial u_z}{\partial x}\right)^2 \\ \dfrac{\partial u_y}{\partial y} + \dfrac{1}{2}\left(\dfrac{\partial u_z}{\partial y}\right)^2 \\ \dfrac{\partial u_y}{\partial x} + \dfrac{\partial u_x}{\partial y} + \dfrac{\partial u_z}{\partial y}\dfrac{\partial u_z}{\partial x} \end{Bmatrix} = \begin{Bmatrix} \varepsilon_{xx}^{(0)} \\ \varepsilon_{yy}^{(0)} \\ \gamma_{xy}^{(0)} \end{Bmatrix} + z\begin{Bmatrix} k_{xx} \\ k_{yy} \\ k_{xy} \end{Bmatrix}$$
$$\begin{Bmatrix} \dfrac{\partial u}{\partial x} + \dfrac{1}{2}\left(\dfrac{\partial w}{\partial x}\right)^2 + \dfrac{\partial w}{\partial x}\dfrac{\partial w^*}{\partial x} \\ \dfrac{\partial v}{\partial y} + \dfrac{1}{2}\left(\dfrac{\partial w}{\partial y}\right)^2 + \dfrac{\partial w}{\partial y}\dfrac{\partial w^*}{\partial y} \\ \dfrac{\partial u}{\partial x} + \dfrac{\partial v}{\partial y} + \dfrac{\partial w}{\partial x}\dfrac{\partial w}{\partial y} + \dfrac{\partial w}{\partial x}\dfrac{\partial w^*}{\partial y} + \dfrac{\partial w}{\partial y}\dfrac{\partial w^*}{\partial x} \end{Bmatrix} - z\begin{Bmatrix} \dfrac{\partial^2 w}{\partial x^2} \\ \dfrac{\partial^2 w}{\partial y^2} \\ 2\dfrac{\partial^2 w}{\partial x \partial y} \end{Bmatrix} \tag{2}$$

To cast light on the opposite small scale effects on the mechanical characteristics of GSs, the authors in the present work introduce the nonlocal strain gradient elasticity theory proposed by Lim *et al*. (2015) which is capable of interpreting the nonlocal effect and the microstructure effect, simultaneously, in the course of analysis. Therefore, the total nonlocal strain gradient stress tensor is given in the following form.

$$(1-\mu^2\nabla^2)\boldsymbol{\sigma} = \boldsymbol{C}:\boldsymbol{\varepsilon} - l^2\nabla\boldsymbol{C}:\nabla\boldsymbol{\varepsilon} \tag{3}$$

in which μ is the nonlocal parameter that is used to capture the significance of nonlocal stress field and l is strain gradient length scale parameter that is used to capture the significance of strain gradient stress field. Besides, $\boldsymbol{C}$ and $\boldsymbol{\varepsilon}$ stand for the fourth-order elasticity tensor and the local strain tensor, separately. Hence, the nonlocal strain gradient constitutive relation of nanoplates can be arrived at employing Eqs. (1) and (2).

$$\begin{aligned} &(1-\mu^2\nabla^2)\begin{Bmatrix} \sigma_{xx} \\ \sigma_{yy} \\ \sigma_{xy} \end{Bmatrix} \\ &= (1-l^2\nabla^2)\begin{pmatrix} \lambda+2\beta & \lambda & 0 \\ \lambda & \lambda+2\beta & 0 \\ 0 & 0 & \beta \end{pmatrix}\begin{Bmatrix} \varepsilon_{xx} \\ \varepsilon_{yy} \\ \varepsilon_{xy} \end{Bmatrix} \end{aligned} \tag{4}$$

Herein, λ and β in Eq. (4) are Lame's constants, the results of which are equal to $Ev/(1\text{-}v^2)$ and $E/[2(1+v)]$ where E and v represent the Young's modulus and the poison's ratio.

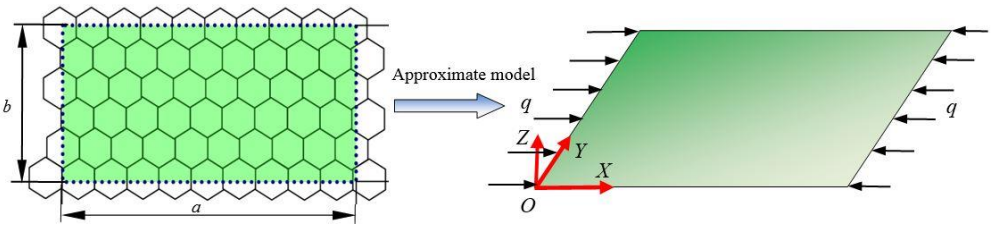

Fig. 1 Schematic view of a graphene sheet under in-plane loading

In the remainder of this section, via using Hamilton's principle (Farokhi and Ghayesh 2017, Farokhi *et al*. 2013, 2016, Farokhi and Ghayesh 2018a, b, Kazemirad *et al*. 2012, Ghayesh 2013, Ghayesh and Moradian 2011, Ghayesh *et al*. 2010, 2011, 2012, 2013a), and then performing the variation of *u*, *v* and *w*, the governing equations of two-dimensional nanoplates can be obtained as

$$\begin{aligned}&\frac{\partial N_{xx}}{\partial x}+\frac{\partial N_{xy}}{\partial y}=0\\&\frac{\partial N_{xy}}{\partial x}+\frac{\partial N_{yy}}{\partial x}=0\\&\frac{\partial^2 M_{xx}}{\partial x^2}+2\frac{\partial^2 M_{xy}}{\partial x\partial y}+\frac{\partial^2 M_{yy}}{\partial y^2}\\&+N_{xx}\frac{\partial^2(w+w^*)}{\partial x^2}+2N_{xy}\frac{\partial^2(w+w^*)}{\partial x\partial y}\\&+N_{yy}\frac{\partial^2(w+w^*)}{\partial y^2}=0\end{aligned}\tag{5}$$

where

$$\begin{aligned}N_{xx}&=\int_{-\frac{h}{2}}^{\frac{h}{2}}\sigma_{xx}dz;\\N_{yy}&=\int_{-\frac{h}{2}}^{\frac{h}{2}}\sigma_{yy}dz;\\N_{xy}&=\int_{-\frac{h}{2}}^{\frac{h}{2}}\sigma_{xy}dz;\\M_{xx}&=\int_{-\frac{h}{2}}^{\frac{h}{2}}z\sigma_{xx}dz;\\M_{yy}&=\int_{-\frac{h}{2}}^{\frac{h}{2}}z\sigma_{yy}dz;\\M_{xy}&=\int_{-h/2}^{h/2}z\sigma_{xy}dz;\end{aligned}$$

Further, the Airy stress function *f*(*x*,*y*) is assumed to be

$$N_{xx}=h\frac{\partial^2 f}{\partial y^2};\quad N_{yy}=h\frac{\partial^2 f}{\partial x^2};\quad N_{xy}=h\frac{\partial^2 f}{\partial x\partial y};\tag{6}$$

Then, through using Eqs. (2) and (6), the geometrical compatibility equation with respect to middle surface strain components of a geometrically imperfect plates can be obtained as

$$\begin{aligned}&\frac{\partial^2\varepsilon_{xx}^{(0)}}{\partial y^2}+\frac{\partial^2\varepsilon_{yy}^{(0)}}{\partial x^2}-\frac{\partial^2\gamma_{xy}^{(0)}}{\partial x\partial y}\\&=\left(\frac{\partial^2 w}{\partial x\partial y}\right)^2-\frac{\partial^2 w}{\partial x^2}\frac{\partial^2 w}{\partial y^2}+2\frac{\partial^2 w}{\partial x\partial y}\frac{\partial^2 w^*}{\partial x\partial y}\\&\quad-\frac{\partial^2 w}{\partial x^2}\frac{\partial^2 w^*}{\partial y^2}-\frac{\partial^2 w}{\partial y^2}\frac{\partial^2 w^*}{\partial x^2}\end{aligned}\tag{7}$$

With the aid of Eqs. (4) and (6), the following non-classical nonlinear governing equations are derived as

$$\begin{aligned}&\frac{\partial^4 f}{\partial y^4}+\frac{\partial^4 f}{\partial x^4}+2\frac{\partial^4 f}{\partial y^2\partial x^2}\\&=E\left[\left(\frac{\partial^2(w+w^*)}{\partial x\partial y}\right)^2-\frac{\partial^2(w+w^*)}{\partial x^2}\cdot\frac{\partial^2(w+w^*)}{\partial y^2}\right]\end{aligned}\tag{8}$$

$$\begin{aligned}&(1-l^2\nabla^2)\left(\frac{\partial^4 w}{\partial x^4}+\frac{\partial^4 w}{\partial y^4}+2\frac{\partial^4 w}{\partial x^2\partial y^2}\right)\\&=\frac{h}{D}(1\\&-\mu^2\nabla^2)\left(\begin{array}{c}\frac{\partial^2 f}{\partial y^2}\frac{\partial^2(w+w^*)}{\partial x^2}+\frac{\partial^2 f}{\partial x^2}\frac{\partial^2(w+w^*)}{\partial y^2}\\-2\frac{\partial^2 f}{\partial x\partial y}\frac{\partial^2(w+w^*)}{\partial x\partial y}\end{array}\right)\end{aligned}\tag{9}$$

where

$$\nabla^2=\frac{\partial^2}{\partial x^2}+\frac{\partial^2}{\partial y^2};D=Eh^3/[12(1-v^2)]$$

In addition, the boundary conditions ought to satisfy the following relations when a two-dimensional plate is subjected to immovable simply supported ends.

$$\begin{aligned}&w=0,\quad M_{xx}=0,\quad N_{xy}=0;\quad at\quad x=0,\\&\text{and}\qquad\int_0^b N_{xx}dy+qbh=0\end{aligned}\tag{10}$$

$$\begin{aligned}&w=0,\quad M_{yy}=0,\quad N_{xy}=0;\quad at\quad y=0,b\\&\text{and}\qquad\int_0^a\int_0^b\frac{\partial V}{\partial y}dxdy=0\end{aligned}\tag{11}$$

Meanwhile, the average end shortening of nanoplate along *X* axis is induced as

$$\begin{aligned}\frac{\Delta x}{a}&=-\frac{1}{ab}\int_0^a\int_0^b\frac{\partial u}{\partial x}dxdy\\&=-\frac{1}{ab}\int_0^a\int_0^b\left[\begin{array}{c}\frac{1}{E}\left(\frac{\partial^2 F}{\partial y^2}-v\frac{\partial^2 F}{\partial x^2}\right)\\-\frac{1}{2}\left(\frac{\partial w}{\partial x}\right)^2-\frac{\partial w}{\partial x}\cdot\frac{\partial w^*}{\partial x}\end{array}\right]dxdy\end{aligned}\tag{12}$$

3. Analytical solution procedure

To acquire the corresponding analytical solutions as clearly and compactly as possible, the following dimensionless parameters are introduced

$$\begin{aligned}&X=\frac{\pi}{a}x;\qquad Y=\frac{\pi}{b}y;\qquad W=\frac{w}{h}\sqrt{12(1-v^2)};\\&W^*=\frac{w^*}{h}\sqrt{12(1-v^2)};\quad \xi=\frac{a}{b};\quad F=\frac{fh}{D};\\&\lambda_q=\frac{qb^2h}{4\pi^2D};\quad \lambda_x=\frac{12(1-v^2)b^2}{4\pi^2h^2}\frac{\Delta x}{a};\\&\bar{l}=\frac{l}{a}\pi;\qquad \bar{\mu}=\frac{\mu}{a}\pi;\end{aligned}$$

Substitution of the above coefficients into Eqs. (8) and

(9) yields the dimensionless governing equations

$$\begin{aligned}&\xi^4\frac{\partial^4 F}{\partial Y^4}+\frac{\partial^4 F}{\partial X^4}+2\xi^2\frac{\partial^4 F}{\partial Y^2\partial X^2}\\&=\xi^2\begin{bmatrix}\left(\frac{\partial^2 W}{\partial X\partial Y}\right)^2-\frac{\partial^2 W}{\partial X^2}\frac{\partial^2 W}{\partial Y^2}+2\frac{\partial^2 W}{\partial X\partial Y}\frac{\partial^2 W^*}{\partial X\partial Y}\\-\frac{\partial^2 W}{\partial X^2}\frac{\partial^2 W^*}{\partial Y^2}-\frac{\partial^2 W}{\partial Y^2}\frac{\partial^2 W^*}{\partial X^2}\end{bmatrix}\end{aligned}\tag{13}$$

$$\begin{aligned}&\frac{\partial^4 W}{\partial X^4}+\xi^4\frac{\partial^4 W}{\partial Y^4}+2\xi^2\frac{\partial^4 W}{\partial X^2\partial Y^2}\\&-\bar{l}^2\begin{pmatrix}\frac{\partial^6 W}{\partial X^6}+3\xi^4\frac{\partial^6 W}{\partial Y^4\partial X^2}\\+3\xi^2\frac{\partial^6 W}{\partial Y^2\partial X^4}+\xi^6\frac{\partial^6 W}{\partial Y^6}\end{pmatrix}\\&=\xi^2\begin{bmatrix}\frac{\partial^2 F}{\partial Y^2}\frac{\partial^2(W+W^*)}{\partial X^2}+\frac{\partial^2 F}{\partial X^2}\frac{\partial^2(W+W^*)}{\partial Y^2}\\-2\frac{\partial^2 F}{\partial X\partial Y}\frac{\partial^2(W+W^*)}{\partial X\partial Y}\\-\bar{\mu}^2\begin{pmatrix}\frac{\partial^2 F}{\partial Y^2}\frac{\partial^4(W+W^*)}{\partial X^4}+\xi^2\frac{\partial^2 F}{\partial Y^2}\frac{\partial^4(W+W^*)}{\partial X^2\partial Y^2}\\+\xi^2\frac{\partial^2 F}{\partial X^2}\frac{\partial^4(W+W^*)}{\partial Y^4}+\frac{\partial^2 F}{\partial X^2}\frac{\partial^4(W+W^*)}{\partial Y^2\partial X^2}\\-2\frac{\partial^2 F}{\partial X\partial Y}\frac{\partial^4(W+W^*)}{\partial Y\partial X^3}-2\xi^2\frac{\partial^2 F}{\partial X\partial Y}\frac{\partial^4(W+W^*)}{\partial Y^3\partial X}\end{pmatrix}\end{bmatrix}\end{aligned}\tag{14}$$

Furthermore, the dimensionless boundary conditions are rewritten as

$$\begin{aligned}&W=\frac{\partial^2 W}{\partial X^2}=0,\quad \frac{\partial^2 F}{\partial X\partial Y}=0;\quad X=0,\pi\\&\text{and}\quad \frac{1}{\pi}\int_0^{\pi}\frac{\partial^2 F}{\partial Y^2}dY+4\lambda_q=0;\\&W=\frac{\partial^2 W}{\partial Y^2}=0,\quad \frac{\partial^2 F}{\partial X\partial Y}=0;\quad Y=0,\pi\\&\text{and}\quad \int_0^{\pi}\int_0^{\pi}\begin{bmatrix}\left(\frac{\partial^2 F}{\partial X^2}-v\xi^2\frac{\partial^2 F}{\partial Y^2}\right)\\-\frac{\xi^2}{2}\left(\frac{\partial W}{\partial Y}\right)^2-\xi^2\frac{\partial W}{\partial Y}\frac{\partial W^*}{\partial Y}\end{bmatrix}dXdY=0\end{aligned}\tag{15}$$

Meanwhile, the dimensionless average end shortening of nanoplate along X axis can be expressed as

$$\lambda_x=-\frac{1}{4\pi^2\xi^2}\int_0^{\pi}\int_0^{\pi}\begin{bmatrix}\left(\xi^2\frac{\partial^2 F}{\partial Y^2}-v\frac{\partial^2 F}{\partial X^2}\right)\\-\frac{1}{2}\left(\frac{\partial W}{\partial X}\right)^2-\frac{\partial W}{\partial X}\frac{\partial W^*}{\partial X}\end{bmatrix}dXdY\tag{16}$$

In the forthcoming part, we utilize the two-step perturbation method to solve the above-derived non-classical governing equations. The two-step perturbation method was proposed via Shen (2013) to study nonlinear mechanical characteristics of structures as well as nanostructures, the advantage of which is capable of providing more accurate analytical solutions compared with those conventional perturbation methods. Differing from the previous researches relevant to this approach, the authors in such work present a new nonlocal strain gradient solution for dimensionless load-deflection curves, the result of which includes the maximum dimensionless deflection to the sixth power. Now, the dimensionless displacement and dimensionless airy stress function can be expanded as

$$\begin{aligned}W(X,Y)&=\sum_{n=1}\varepsilon^n W_n(X,Y);\ F(X,Y)\\&=\sum_{n=1}\varepsilon^n F_n(X,Y);\end{aligned}\tag{17}$$

where ε is only the small perturbation parameter that has no physical meaning in step-by-step procedure. And, we suppose that the initial dimensionless displacement of geometrically imperfect plate is similar to that of perfect plate.

$$\begin{aligned}W^*&=\varepsilon A_{11}^*\sin(mX)\sin(nY)\\&=\varepsilon\eta A_{11}^{(1)}\sin(mX)\sin(nY)\end{aligned}\tag{18}$$

in which η represents the imperfection parameter that is $\eta=A_{11}^*/A_{11}^{(1)}$. We substitute Eq. (17) into Eqs. (13) and (14), and then to collect the same order ε so that a series of perturbation equations are listed as

$$\begin{aligned}&O(\varepsilon^1)\\&\frac{\partial^4 F_1}{\partial X^4}+2\xi^2\frac{\partial^4 F_1}{\partial Y^2\partial X^2}+\xi^4\frac{\partial^4 F_1}{\partial Y^4}=0\end{aligned}\tag{19}$$

$$\begin{aligned}&\frac{\partial^4 W_1}{\partial X^4}+\xi^4\frac{\partial^4 W_1}{\partial Y^4}+2\xi^2\frac{\partial^4 W_1}{\partial X^2\partial Y^2}\\&-\bar{l}^2\begin{pmatrix}\frac{\partial^6 W_1}{\partial X^6}+3\xi^4\frac{\partial^6 W_1}{\partial Y^4\partial X^2}\\+3\xi^2\frac{\partial^6 W_1}{\partial Y^2\partial X^4}+\xi^6\frac{\partial^6 W_1}{\partial Y^6}\end{pmatrix}\\&=\xi^2\begin{bmatrix}\frac{\partial^2 F_0}{\partial Y^2}\frac{\partial^2(W_1+W^*)}{\partial X^2}+\frac{\partial^2 F_0}{\partial X^2}\frac{\partial^2(W_1+W^*)}{\partial Y^2}\\-2\frac{\partial^2 F_0}{\partial X\partial Y}\frac{\partial^2(W_1+W^*)}{\partial X\partial Y}\\-\bar{\mu}^2\begin{pmatrix}\frac{\partial^2 F_0}{\partial Y^2}\frac{\partial^4(W_0+W^*)}{\partial X^4}\\+\xi^2\frac{\partial^2 F_0}{\partial Y^2}\frac{\partial^4(W_1+W^*)}{\partial X^2\partial Y^2}\\+\xi^2\frac{\partial^2 F_0}{\partial X^2}\frac{\partial^4(W_1+W^*)}{\partial Y^4}\\+\frac{\partial^2 F_0}{\partial X^2}\frac{\partial^4(W_1+W^*)}{\partial Y^2\partial X^2}\\-2\frac{\partial^2 F_0}{\partial X\partial Y}\frac{\partial^4(W_1+W^*)}{\partial Y\partial X^3}\\-2\xi^2\frac{\partial^2 F_0}{\partial X\partial Y}\frac{\partial^4(W_1+W^*)}{\partial Y^3\partial X}\end{pmatrix}\end{bmatrix}\end{aligned}\tag{20}$$

$$\begin{aligned}&O(\varepsilon^2)\\&\xi^4\frac{\partial^4 F_2}{\partial Y^4}+\frac{\partial^4 F_2}{\partial X^4}+2\xi^2\frac{\partial^4 F_2}{\partial Y^2\partial X^2}\\&=\xi^2\begin{bmatrix}\left(\frac{\partial^2 W_1}{\partial X\partial Y}\right)^2-\frac{\partial^2 W_1}{\partial X^2}\frac{\partial^2 W_1}{\partial Y^2}+2\frac{\partial^2 W_1}{\partial X\partial Y}\frac{\partial^2 W^*}{\partial X\partial Y}\\-\frac{\partial^2 W_1}{\partial X^2}\frac{\partial^2 W^*}{\partial Y^2}-\frac{\partial^2 W_1}{\partial Y^2}\frac{\partial^2 W^*}{\partial X^2}\end{bmatrix}\end{aligned}\tag{21}$$

$$\begin{aligned}
&\frac{\partial^4 W_2}{\partial X^4}+\xi^4\frac{\partial^4 W_2}{\partial Y^4}+2\xi^2\frac{\partial^4 W_2}{\partial X^2\partial Y^2}\\
&-\bar{l}^2\left(\frac{\partial^6 W_2}{\partial X^6}+3\xi^4\frac{\partial^6 W_2}{\partial Y^4\partial X^2}+3\xi^2\frac{\partial^6 W_2}{\partial Y^2\partial X^4}+\xi^6\frac{\partial^6 W_2}{\partial Y^6}\right)\\
&=\xi^2\begin{bmatrix}\dfrac{\partial^2 F_0}{\partial Y^2}\dfrac{\partial^2 W_2}{\partial X^2}+\dfrac{\partial^2 F_0}{\partial X^2}\dfrac{\partial^2 W_2}{\partial Y^2}\\ -2\dfrac{\partial^2 F_0}{\partial X\partial Y}\dfrac{\partial^2 W_2}{\partial X\partial Y}\\ -2\dfrac{\partial^2 F_0}{\partial X\partial Y}\dfrac{\partial^2 W_2}{\partial X\partial Y}\\ -\bar{\mu}^2\begin{pmatrix}\dfrac{\partial^2 F_0}{\partial Y^2}\dfrac{\partial^4 W_2}{\partial X^4}+\xi^2\dfrac{\partial^2 F_0}{\partial Y^2}\dfrac{\partial^4 W_2}{\partial X^2\partial Y^2}\\ +\xi^2\dfrac{\partial^2 F_0}{\partial X^2}\dfrac{\partial^4 W_2}{\partial Y^4}+\dfrac{\partial^2 F_0}{\partial X^2}\dfrac{\partial^4 W_2}{\partial Y^2\partial X^2}\\ -2\dfrac{\partial^2 F_0}{\partial X\partial Y}\dfrac{\partial^4 W_2}{\partial Y\partial X^3}-2\xi^2\dfrac{\partial^2 F_0}{\partial X\partial Y}\dfrac{\partial^4 W_2}{\partial Y^3\partial X}\end{pmatrix}\end{bmatrix}
\end{aligned}\tag{22}$$

$$O(\varepsilon^3)$$

$$\begin{aligned}
&\xi^4\frac{\partial^4 F_3}{\partial Y^4}+\frac{\partial^4 F_3}{\partial X^4}+2\xi^2\frac{\partial^4 F_3}{\partial Y^2\partial X^2}\\
&=\xi^2\begin{bmatrix}2\dfrac{\partial^2 W_1}{\partial X\partial Y}\dfrac{\partial^2 W_2}{\partial X\partial Y}-\dfrac{\partial^2 W_2}{\partial X^2}\dfrac{\partial^2 W_1}{\partial Y^2}-\dfrac{\partial^2 W_1}{\partial X^2}\dfrac{\partial^2 W_2}{\partial Y^2}\\ +2\dfrac{\partial^2 W_2}{\partial X\partial Y}\dfrac{\partial^2 W^*}{\partial X\partial Y}-\dfrac{\partial^2 W_2}{\partial X^2}\dfrac{\partial^2 W^*}{\partial Y^2}-\dfrac{\partial^2 W_2}{\partial Y^2}\dfrac{\partial^2 W^*}{\partial X^2}\end{bmatrix}
\end{aligned}\tag{23}$$

$$\begin{aligned}
&\frac{\partial^4 W_3}{\partial X^4}+\xi^4\frac{\partial^4 W_3}{\partial Y^4}+2\xi^2\frac{\partial^4 W_3}{\partial X^2\partial Y^2}\\
&-\bar{l}^2\begin{pmatrix}\dfrac{\partial^6 W_3}{\partial X^6}+3\xi^4\dfrac{\partial^6 W_3}{\partial Y^4\partial X^2}\\ +3\xi^2\dfrac{\partial^6 W_3}{\partial Y^2\partial X^4}+\xi^6\dfrac{\partial^6 W_3}{\partial Y^6}\end{pmatrix}\\
&=\xi^2\begin{bmatrix}\dfrac{\partial^2 F_0}{\partial Y^2}\dfrac{\partial^2 W_3}{\partial X^2}+\dfrac{\partial^2 F_0}{\partial X^2}\dfrac{\partial^2 W_3}{\partial Y^2}\\ -2\dfrac{\partial^2 F_0}{\partial X\partial Y}\dfrac{\partial^2 W_3}{\partial X\partial Y}+\dfrac{\partial^2 F_2}{\partial Y^2}\dfrac{\partial^2 (W_1+W^*)}{\partial X^2}\\ +\dfrac{\partial^2 F_2}{\partial X^2}\dfrac{\partial^2 (W_1+W^*)}{\partial Y^2}\\ -2\dfrac{\partial^2 F_2}{\partial X\partial Y}\dfrac{\partial^2 (W_1+W^*)}{\partial X\partial Y}\end{bmatrix}\\
&-\xi^2\bar{\mu}^2\begin{pmatrix}\dfrac{\partial^2 F_0}{\partial Y^2}\dfrac{\partial^4 W_3}{\partial X^4}+\xi^2\dfrac{\partial^2 F_0}{\partial Y^2}\dfrac{\partial^4 W_3}{\partial X^2\partial Y^2}\\ -2\dfrac{\partial^2 F_0}{\partial X\partial Y}\dfrac{\partial^4 W_3}{\partial Y\partial X^3}\\ -2\xi^2\dfrac{\partial^2 F_0}{\partial X\partial Y}\dfrac{\partial^4 W_3}{\partial Y^3\partial X}\dfrac{\partial^2 F_2}{\partial Y^2}\dfrac{\partial^4 (W_1+W^*)}{\partial X^4}\\ +\xi^2\dfrac{\partial^2 F_2}{\partial Y^2}\dfrac{\partial^4 (W_1+W^*)}{\partial X^2\partial Y^2}\\ +\xi^2\dfrac{\partial^2 F_2}{\partial X^2}\dfrac{\partial^4 (W_1+W^*)}{\partial Y^4}\\ +\dfrac{\partial^2 F_2}{\partial X^2}\dfrac{\partial^4 (W_1+W^*)}{\partial Y^2\partial X^2}\\ -2\dfrac{\partial^2 F_2}{\partial X\partial Y}\dfrac{\partial^4 (W_1+W^*)}{\partial Y\partial X^3}\\ -2\xi^2\dfrac{\partial^2 F_2}{\partial X\partial Y}\dfrac{\partial^4 (W_1+W^*)}{\partial Y^3\partial X}\end{pmatrix}
\end{aligned}\tag{24}$$

In the present case, asymptotic solutions of dimensionless displacement and dimensionless airy stress function which satisfy simply supported boundary conditions are set as

$$\begin{aligned}
W&=\varepsilon A_{11}^{(1)}\sin(mX)\sin(nY)\\
&\quad+\varepsilon^3\begin{bmatrix}A_{13}^{(3)}\sin(mX)\sin(3nY)\\ +A_{31}^{(3)}\sin(3mX)\sin(nY)\end{bmatrix}+O(\varepsilon^5)\\
F&=-B_{00}^{(0)}\frac{Y^2}{2}-b_{00}^{(0)}\frac{X^2}{2}\\
&\quad+\varepsilon^2\begin{bmatrix}-B_{00}^{(2)}\dfrac{Y^2}{2}-b_{00}^{(2)}\dfrac{X^2}{2}\\ +B_{20}^{(2)}\cos(2mX)\\ +B_{02}^{(2)}\cos(2nY)\end{bmatrix}+O(\varepsilon^4)
\end{aligned}\tag{25}$$

Via submitting Eq. (25) into Eq. (15), one has

$$\lambda_q=\frac{1}{4}\left(B_{00}^{(0)}+\varepsilon^2 B_{00}^{(2)}+\dots\right)\tag{26}$$

Similarly, through submitting Eq. (25) into Eq. (16), the average end shortening of plate can be given as

$$\begin{aligned}
\lambda_x&=\frac{1}{4\xi^2}\begin{bmatrix}\xi^2 B_{00}^{(0)}+\xi^2 B_{00}^{(2)}+\cdots\\ -v\left(b_{00}^{(0)}+b_{00}^{(2)}+\cdots\right)\end{bmatrix}\\
&+\frac{m^2(1+2\eta)}{32\xi^2}\left[A_{11}^{(1)}\right]^2+\frac{m^2}{32\xi^2}\left[A_{13}^{(3)}\right]^2\\
&+\frac{9m^2}{32\xi^2}\left[A_{31}^{(3)}\right]^2+\cdots
\end{aligned}\tag{27}$$

In order to determine the relations among the parameters of Eqs. (26) and (27), we perform some mathematical operations for the above-obtained perturbation equations. The substitution of Eq. (25) into Eq. (20) yields

$$\begin{aligned}
&\xi^2\left(B_{00}^{(0)}m^2+b_{00}^{(0)}n^2\right)\\
&=\frac{(m^2+n^2\xi^2)^2\left[1+\bar{l}^2(m^2+\xi^2n^2)\right]}{(1+\eta)[1+\bar{\mu}^2(m^2+\xi^2n^2)]}
\end{aligned}\tag{28}$$

Then substituting Eq. (25) into Eq. (21), one has

$$\begin{aligned}
B_{20}^{(2)}&=\frac{n^2\xi^2}{32m^2}(1+2\eta)\left[A_{11}^{(1)}\right]^2;\\
B_{02}^{(2)}&=\frac{m^2}{32n^2\xi^2}(1+2\eta)\left[A_{11}^{(1)}\right]^2;
\end{aligned}\tag{29}$$

After we submitting Eq. (25) into Eq. (24) having

$$\begin{aligned}
&A_{31}^3\sin(3mx)\sin(ny)\begin{Bmatrix}\left(\dfrac{9m^2}{+n^2\xi^2}\right)^2\left[1+\bar{l}^2\left(\dfrac{9m^2}{+n^2\xi^2}\right)\right]\\ -\left(\dfrac{9m^2B_{00}^{(0)}}{+n^2b_{00}^{(0)}}\right)\xi^2\left[1+\bar{\mu}^2\left(\dfrac{9m^2}{+n^2\xi^2}\right)\right]\end{Bmatrix}\\
&+A_{13}^3\sin(mx)\sin(3ny)\begin{Bmatrix}\left(\dfrac{m^2}{+9n^2\xi^2}\right)^2\left[1+\bar{l}^2\left(\dfrac{m^2}{+9n^2\xi^2}\right)\right]\\ -\left(\dfrac{m^2B_{00}^{(0)}}{+9n^2b_{00}^{(0)}}\right)\xi^2\left[1+\bar{\mu}^2\left(\dfrac{m^2}{+9n^2\xi^2}\right)\right]\end{Bmatrix}\\
&=\xi^2(1+\eta)\begin{bmatrix}1+\bar{\mu}^2(m^2\\ +n^2\xi^2)\end{bmatrix}\begin{Bmatrix}A_{11}^{(1)}\sin(mx)\sin(ny)\begin{bmatrix}m^2B_{00}^{(2)}+n^2b_{00}^{(2)}\\ -2m^2n^2\left(B_{02}^{(2)}+B_{20}^{(2)}\right)\end{bmatrix}\\ +2m^2n^2B_{02}^{(2)}A_{11}^{(1)}\sin(3ny)\sin(mx)\\ +2m^2n^2B_{20}^{(2)}A_{11}^{(1)}\sin(ny)\sin(3mx)\end{Bmatrix}
\end{aligned}\tag{30}$$

From Eq. (30), we can derive the following relations.

$$m^2 B_{00}^{(2)} + n^2 b_{00}^{(2)} = \frac{(1+2\eta)(m^4+n^4\xi^4)}{16\xi^2}\left[A_{11}^{(1)}\right]^2 \quad (31)$$

and

$$A_{13}^3 = \frac{m^4(1+2\eta)(1+\eta)}{16\begin{Bmatrix}(m^2+9n^2\xi^2)^2\left[1+\bar{l}^2(m^2+9n^2\xi^2)\right]\\ -(m^2B_{00}^{(0)}+9n^2b_{00}^{(0)})\xi^2[1+\bar{\mu}^2(m^2+9n^2\xi^2)]\end{Bmatrix}}\left[1+\bar{\mu}^2(m^2+n^2\xi^2)\right]\left[A_{11}^{(1)}\right]^3$$
$$A_{31}^3 = \frac{\xi^4 n^4(1+2\eta)(1+\eta)}{16\begin{Bmatrix}(9m^2+n^2\xi^2)^2\left[1+\bar{l}^2(9m^2+n^2\xi^2)\right]\\ -(9m^2B_{00}^{(0)}+n^2b_{00}^{(0)})\xi^2[1+\bar{\mu}^2(9m^2+n^2\xi^2)]\end{Bmatrix}}\left[1+\bar{\mu}^2(m^2+n^2\xi^2)\right]\left[A_{11}^{(1)}\right]^3 \quad (32)$$

Obviously, $A_{11}^{(1)}$ is considered as the second perturbation parameter and related to the maximum dimensionless deflection when $X = \pi/2m$, $Y = \pi/2n$. Consequently, the analytical solution of the maximum dimensionless deflection W_m can be written as, using the first equation of Eq. (25).

$$W_m = A_{11}^{(1)}\varepsilon - (A_{13}^{(3)} + A_{31}^{(3)})\varepsilon^3 + O(\varepsilon^5) \quad (33)$$

Rather, $A_{11}^{(1)}$ can be expressed as

$$A_{11}^{(1)}\varepsilon = W_m + K(W_m)^3 \quad (34)$$

where

$$K = \frac{1}{16}(1+\eta)^2(1+2\eta)\begin{Bmatrix}\dfrac{m^4 a_1 a_2^2}{a_3 a_2 a_5^2 a_1(1+\eta) - a_6 a_7 a_8 a_9^2}\\ +\dfrac{\xi^4 n^4 a_1 a_2^2}{a_{10} a_2 a_{11}^2 a_1(1+\eta) - a_{12} a_6 a_4 a_9^2}\end{Bmatrix}(W_m)^3$$

in which

$$\begin{aligned}
a_1 &= m^2 + \nu n^2\xi^2;\\
a_5 &= m^2 + 9n^2\xi^2;\\
a_8 &= 9\nu n^2\xi^2 + m^2;\\
a_{11} &= 9m^2 + n^2\xi^2;\\
a_2 &= 1 + \bar{\mu}^2(m^2+n^2\xi^2);\\
a_6 &= 1 + \bar{l}^2(m^2+n^2\xi^2);\\
a_9 &= m^2 + n^2\xi^2;\\
a_{12} &= 1 + \bar{\mu}^2(9m^2+n^2\xi^2);\\
a_3 &= 1 + \bar{l}^2(m^2+9n^2\xi^2);\\
a_7 &= 1 + \bar{\mu}^2(m^2+9n^2\xi^2);\\
a_{10} &= 1 + \bar{l}^2(9m^2+n^2\xi^2);\\
a_4 &= 9m^2 + \nu n^2\xi^2;
\end{aligned}$$

The substitution of Eq. (25) into the second equation of Eq. (15) yields

$$\begin{aligned}
&-\left(b_{00}^0 + \varepsilon^2 b_{00}^{(2)} + \cdots\right) + \nu\xi^2\left(B_{00}^0 + \varepsilon^2 B_{00}^{(2)} + \cdots\right)\\
&-\varepsilon^2(1+2\eta)\frac{n^2\xi^2}{8}\left[A_{11}^{(1)}\right]^2 - \varepsilon^6\frac{9}{8}n^2\xi^2\left[A_{13}^{(3)}\right]^2\\
&-\varepsilon^6\frac{1}{8}n^2\xi^2\left[A_{31}^{(3)}\right]^2 + \ldots = 0
\end{aligned} \quad (35)$$

When ε is close to zero, the relationship between $B_{00}^{(0)}$ and $b_{00}^{(0)}$ in Eq. (35) should be satisfied as

$$-b_{00}^{(0)} + \nu\xi^2 B_{00}^{(0)} = 0 \quad (36)$$

Then, using Eqs. (28) and (36), we have

$$B_{00}^{(0)} = \frac{(m^2+n^2\xi^2)^2\left[1+\bar{l}^2(m^2+n^2\xi^2)\right]}{(1+\eta)\xi^2(m^2+\nu n^2\xi^2)[1+\bar{\mu}^2(m^2+n^2\xi^2)]} \quad (37)$$

By employing the principle of superposition for Eqs. (28), (31) and (35), Eq. (26) can be changed into another form.

$$\begin{aligned}
\lambda_q &= \frac{1}{4}\left(B_{00}^{(0)} + \varepsilon^2 B_{00}^{(2)} + \ldots\right)\\
&= \frac{1}{4(m^2+\nu n^2\xi^2)\xi^2}\begin{Bmatrix}\dfrac{(m^2+n^2\xi^2)^2\left[1+\bar{l}^2(m^2+n^2\xi^2)\right]}{(1+\eta)[1+\bar{\mu}^2(m^2+n^2\xi^2)]}\\ +\varepsilon^2\dfrac{1}{16}(1+2\eta)(m^4+3n^4\xi^4)\left[A_{11}^{(1)}\right]^2\\ \varepsilon^6\dfrac{1}{8}n^4\xi^4[9(A_{13}^3)^2 + (A_{31}^3)^2] + \ldots\end{Bmatrix}
\end{aligned} \quad (38)$$

Finally, via submitting Eqs. (32) and (34) into Eq. (38), the expression of λ_q can be expressed as

$$\begin{aligned}
\lambda_q &= k_0\left(\frac{W_m}{h}\right)^0 + k_2\left(\frac{W_m}{h}\right)^2\\
&+ k_4\left(\frac{W_m}{h}\right)^4 + k_6\left(\frac{W_m}{h}\right)^6 + \cdots
\end{aligned} \quad (39)$$

in which

$$\begin{aligned}
k_0 &= \frac{(m^2+n^2\xi^2)^2\left[1+\bar{l}^2(m^2+n^2\xi^2)\right]}{4\xi^2(1+\eta)(m^2+\nu n^2\xi^2)[1+\bar{\mu}^2(m^2+n^2\xi^2)]};\\
k_2 &= \frac{3(1+2\eta)(m^4+3n^4\xi^4)(1-\nu^2)}{16\xi^2(m^2+\nu n^2\xi^2)};\\
k_4 &= \frac{(1+2\eta)^2(m^4+3n^4\xi^4)}{[12(1-\nu^2)]^2(1+\eta)^2}\begin{Bmatrix}\dfrac{m^4 a_1 a_2^2}{a_3 a_2 a_5^2 a_1(1+\eta)}\\ -a_6 a_7 a_8 a_9^2\\ +\dfrac{\eta^4 n^4 a_1 a_2^2}{a_{10} a_2 a_{11}^2 a_1(1+\eta)}\\ -a_{12} a_6 a_4 a_9^2\end{Bmatrix};\\
k_6 &= \left[\frac{32k_4\xi^2(m^2+\nu n^2\xi^2)}{(m^4+3n^4\xi^4)}\right]^2[12(1-\nu^2)]^3\\
&\quad \frac{(1+2\eta)(m^4+3n^4\xi^4)}{64\xi^2(m^2+\nu n^2\xi^2)} + \frac{n^4\xi^4[12(1-\nu^2)]^3}{32\xi^2(m^2+\nu n^2\xi^2)}\\
&\quad \begin{Bmatrix}\dfrac{9}{256}\left[\dfrac{(1+2\eta)(1+\eta)^2}{a_3 a_2 a_5^2 a_1(1+\eta)}\right]^2\\ -a_6 a_7 a_8 a_9^2\\ +\dfrac{1}{256}\left[\dfrac{(1+2\eta)(1+\eta)^2}{a_{10} a_2 a_{11}^2 a_1(1+\eta)}\right]^2\\ -a_{12} a_6 a_4 a_9^2\end{Bmatrix}
\end{aligned}$$

Similarly, by employing the principle of superposition for the average end shortening of plate, Eq. (27) can be changed into another form.

$$\lambda_x = (1-v^2)\lambda_q + \frac{(1+2\eta)}{32\xi^2}(m^2+vn^2\xi^2)\left[A_{11}^{(1)}\right]^2 + \frac{(m^2+9vn^2\xi^2)}{32\xi^2}\left[A_{13}^{(3)}\right]^2 + \frac{(9m^2+vn^2\xi^2)}{32\xi^2}\left[A_{31}^{(3)}\right]^2 \ldots \quad (40)$$

Ulteriorly, by submitting Eqs. (32), (34) and (39) into Eq. (40), the expression of λ_x can be expressed as

$$\lambda_x = (1-v^2)\lambda_q + g_2\left(\frac{w_m}{h}\right)^2 + g_4\left(\frac{w_m}{h}\right)^4 + g_6\left(\frac{w_m}{h}\right)^6 \ldots \quad (41)$$

in which

$$g_2 = \frac{3}{8\xi^2}(1-v^2)(1+2\eta)(m^2+vn^2\xi^2);$$

$$g_4 = \frac{2k_4(m^2+vn^2\xi^2)^2}{(m^4+3n^4\xi^4)};$$

$$g_6 = 12(1-v^2)\frac{k_4(m^2+vn^2\xi^2)^2}{(m^4+3n^4\xi^4)} + [12(1-v^2)]^3\frac{(m^2+9vn^2\xi^2)}{32\xi^2}\left[\frac{m^4a_1a_2^2(1+\eta)^2(1+2\eta)}{16[a_3a_2a_5^2a_1(1+\eta)-a_6a_7a_8a_9^2]}\right]^2 + [12(1-v^2)]^3\frac{(9m^2+vn^2\xi^2)}{32\xi^2}\left[\frac{\xi^4n^4a_1a_2^2(1+\eta)^2(1+2\eta)}{16[a_{10}a_2a_{11}^2a_1(1+\eta)-a_{12}a_6a_4a_9^2]}\right]^2$$

Although the authors in this section for the first time present the approximated analytical solutions of λ_q and λ_x that include the maximum dimensionless flexural deflection to the sixth power, as shown in Figs. 2 and 3, there is no significant difference between the solutions to the sixth power and the solutions to the forth power in predicting the responses of a single-layer graphene. Thus, in the forthcoming section, unless noted otherwise, the Eqs. (42) and (43) are used to investigate the axial buckling and post-buckling of a single-layer graphene.

$$\lambda_q = k_0\left(\frac{w_m}{h}\right)^0 + k_2\left(\frac{w_m}{h}\right)^2 + k_4\left(\frac{w_m}{h}\right)^4 + \cdots \quad (42)$$

$$\lambda_x = (1-v^2)\lambda_q + g_2\left(\frac{w_m}{h}\right)^2 + g_4\left(\frac{w_m}{h}\right)^4 + \cdots \quad (43)$$

Before performing the analysis of the influence of various parameters on the axial buckling and post-buckling of single layer graphene sheets, we should undertake several validation researches to conform the accuracy of the present analytical solutions. For this purpose, as indicated in Table. 1, we present the comparison of dimensionless critical buckling loads of perfect rectangular graphene sheets subjected to uniform in-plane compression loading, where the dimensionless critical buckling load is defined as$\bar{P} = Pa^2/D$. Meanwhile, the postbuckling load-deflection curve for a perfect isotropic thin plate subjected to uniaxial compression is compared in Fig. 4 with the solution of Shen (2013). It is found from the table and the figure that there is

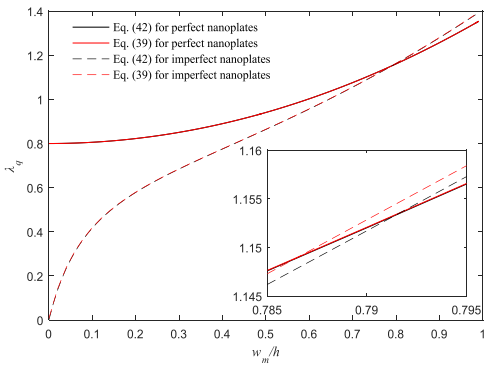

Fig. 2 Comparison of dimensionless post-buckling load–deflection curves of perfect and imperfect GSs using different approximated analytical solutions

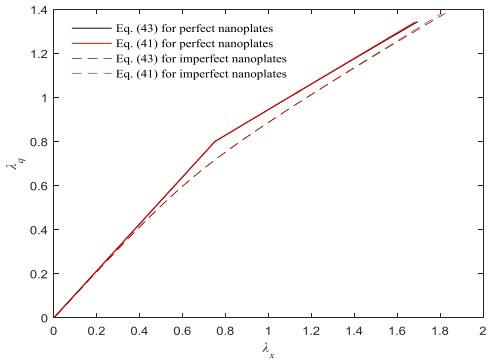

Fig. 3 Comparison of dimensionless post-buckling load-shortening curves of perfect and imperfect GSs using different approximated analytical solutions

Table 1 Comparison of dimensionless buckling loads of rectangular graphene sheets subjected to uniform in-plane compressive loading

$(ea)^2$ ((nm)^2)	Present	Hashemi and Samaei (2011)	Difference	Pradhan (2009)	Difference	Pradhan and Murmu (2009)	Difference
0	9.8696	9.867	0.0264%	9.8671	0.0253%	9.8791	0.0963%
0.5	9.40547	9.4029	0.0273%	9.4031	0.0252%	9.4156	0.1077%
1	8.98302	8.9803	0.0303%	8.9807	0.0258%	8.9947	0.1300%
1.5	8.59697	8.5939	0.0357%	8.5947	0.0264%	8.6073	0.1202%
2	8.24261	8.2393	0.0402%	8.2405	0.0256%	8.2537	0.1345%

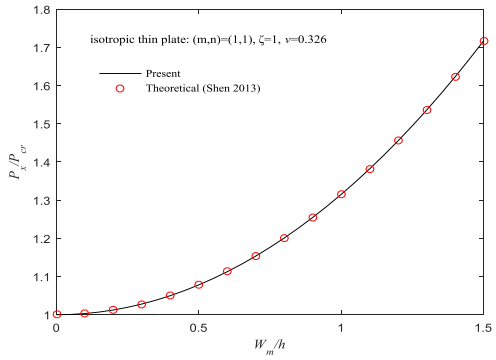

Fig. 4 Comparison of postbuckling load–deflection curves for a perfect isotropic plate

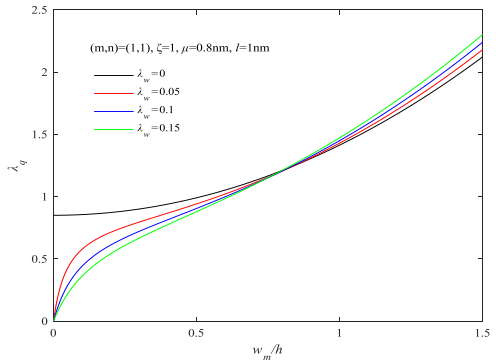

Fig. 5 Comparison of dimensionless post-buckling load–deflection curves of perfect and imperfect GSs

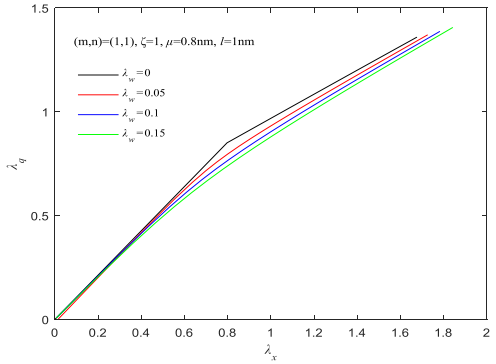

Fig. 6 Comparison of dimensionless post-buckling load-shortening curves of perfect and imperfect GSs

an absolutely reasonable agreement between the results obtained by the current solution and the ones predicted by Hashemi and Samaei (2011), Pradhan (2009), Pradhan and Murmu (2009) and Shen (2013), which can ensure the validity and the reliability of the present analysis.

Next, the main aim of the rest of section is to provide a parametric investigation to reveal the effects of nonlocal parameters, strain gradient parameters, geometrical imperfection as well as mode numbers on axial-buckling and post-buckling of geometrically imperfect single-layer graphene sheets. The physical material properties are listed here: v = 0.25, E = 1.06 Tpa, h = 0.34 nm, a = 10 nm. Furthermore, the value range of the nonlocal parameter μ and the stain gradient parameter l is set at 0 to 2 nm, because the exact value of the nonlocal parameter μ can't be predicted accurately (Wang 2005) and what both the theoretical study and the experimental study conducted by Ma *et al.* (2008) and Mcfarland and Colton (2005) are indicating is that there exists a significant size-dependent relation between the value of the strain gradient parameter l and the thickness of structural components.

Fig. 5 shows the comparison of dimensionless post-buckling load-deflection curves of perfect and imperfect GSs, where λ_w is the maximum dimensionless initial geometric imperfection that is denoted as $\lambda_w = w_m^*/h$, and a imperfect plate is degenerated into a perfect plate at λ_w = 0. It is interesting to note from this figure that unlike for the imperfect GSs, there exists no deflection in the pre-buckling domain of the perfect GSs. Besides, the difference between the imperfect GSs and the perfect GSs enhances, first, but then reduces with the dimensionless deflection becoming bigger and bigger. Meanwhile, Fig. 6 shows the comparison of dimensionless post-buckling load-shortening curves of perfect and imperfect GSs. It is found form the figure that the imperfect GSs under axial compressions produce dimensionless post-buckling load-shortening curves appearing smooth and monotonous, compared with those of the perfect GSs. Besides, the increment of the dimensionless initial geometric imperfection tends to reduce the effective stiffness of components. Consequently, in view of foregoing analyses, the initial geometric imperfection plays a significant role in predicting the response of structural components subjected to loading conditions.

Fig. 7 presents the effect of nonlocal parameters on the dimensionless post-buckling load–deflection curves of perfect and imperfect GSs and Fig. 8 presents the effect of nonlocal parameters on the dimensionless post-buckling load–shortening curves of perfect and imperfect GSs. As shown in the figures, for the perfect GSs and the imperfect GSs, the increase of the nonlocal parameter results in a decrease in the value of the critical buckling load and the critical end-shortening. In other words, the nonlocal parameter is capable of reducing the effective stiffness of nanostructures. Furthermore, the rise of the nonlocal parameter decreases the slope of post-buckling part of load-

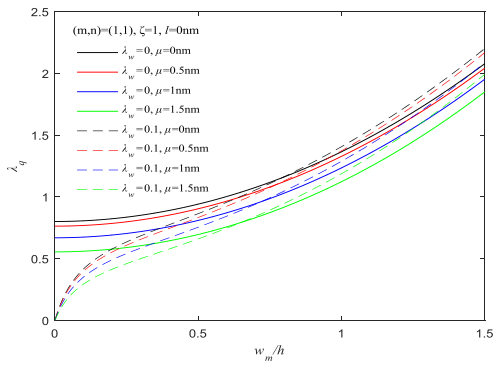

Fig. 7 Effect of nonlocal parameters on the dimensionless post-buckling load–deflection curves of perfect and imperfect GSs

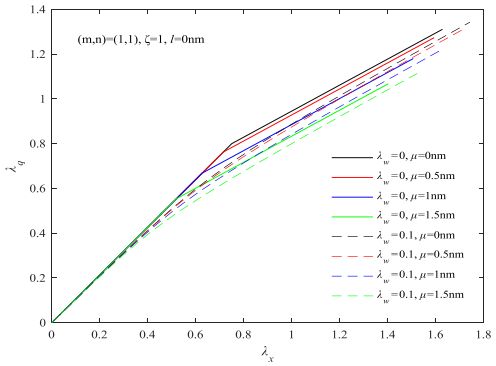

Fig. 8 Effect of nonlocal parameters on the dimensionless post-buckling load–shortening curves of perfectand imperfect GSs

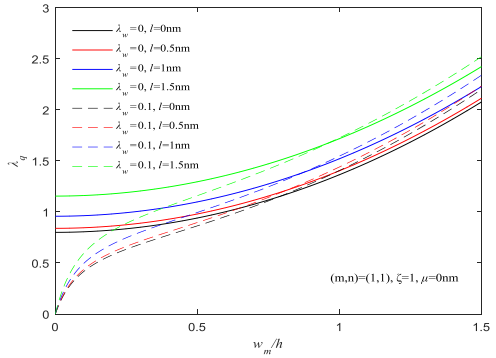

Fig. 9 Effect of strain gradient parameters on the dimensionless post-buckling load–deflection curves of perfect and imperfect GSs

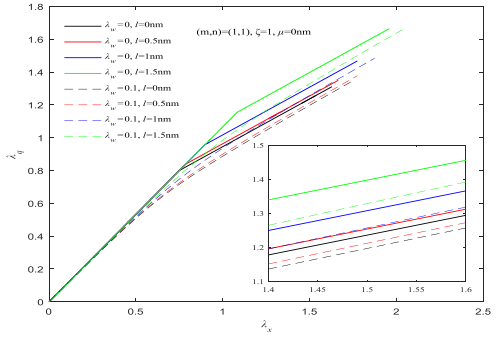

Fig. 10 Effect of strain gradient parameters on the dimensionless post-buckling load–shortening curves of perfect and imperfect GSs

shortening curve, regardless of which type of graphene sheets.

Fig. 9 presents the effect of strain gradient parameters on the dimensionless post-buckling load–deflection curves of perfect and imperfect GSs and Fig. 10 presents the effect of the strain gradient parameter on the dimensionless post-buckling load–shortening curves of perfect and imperfect GSs. As shown in the figures, for the perfect GSs and the imperfect GSs, the increase of the strain gradient parameter leads to an increase in the value of the critical buckling load

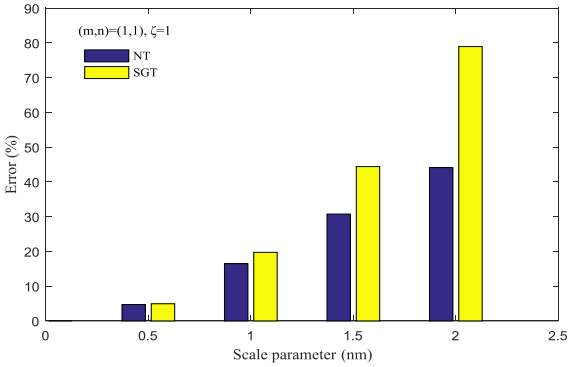

Fig. 11 Error of the classical model in prediction of critical buckling load of perfect GSs

and the critical end-shortening. That is, the stain gradient parameter can improve the effective stiffness of nanostructures. Moreover, the rise of the stain gradient parameter makes the slope of post-buckling part of load-shortening curve bigger, regardless of which type of graphene sheets.

Fig. 11 displays the error of the classical model in prediction of critical buckling load of perfect GSs, where NT and SGT respectively stand for the nonlocal elasticity theory and the strain gradient theory, and the formulation of the error is denoted as

$$\text{Error}(\%) = \left| \frac{\text{classical buckling load} - \text{nonclassical buckling load}}{\text{classical bucklingload}} \right| \times 100\% \qquad (44)$$

It is indicated from the above figure that the size-dependent effect becomes more prominent with the results of the nonlocal parameter and the strain gradient parameter increasing progressively so that the error of the classical model continues to ascend in predicting the critical buckling load of perfect GSs. Thus, the size-dependent effect can't be ignored in analysis of nonlinear instability of nanostructures.

Figs. 12 and 13 respectively show the comparison of size-dependent dimensionless post-buckling load-deflection

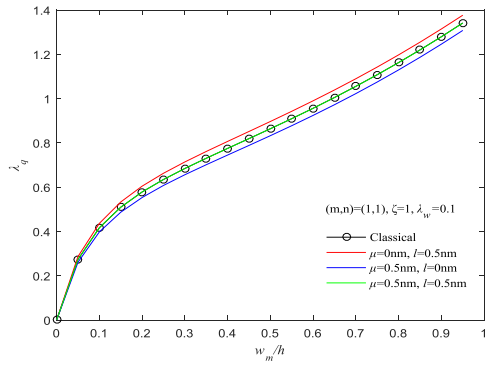

Fig. 12 Comparison of size-dependent dimensionless post-buckling load–deflection curves of imperfect GSs in the framework of nonlocal strain gradient elasticity theory

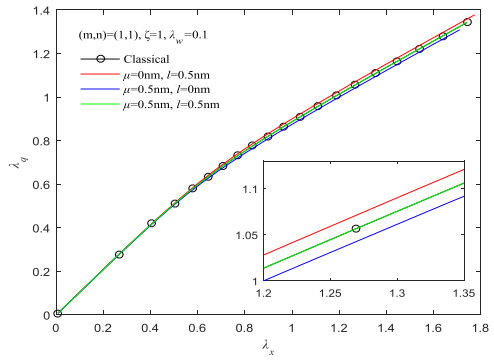

Fig. 13 Comparison of size-dependent dimensionless post-buckling load–shortening curves of imperfect GSs in the frameworkof nonlocal strain gradient elasticity theory

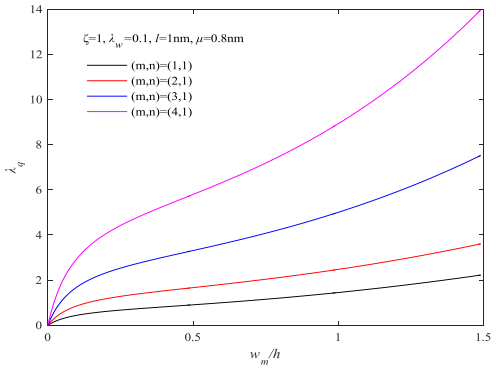

Fig. 14 Dimensionless post-buckling load–deflection curves of imperfect GSs with the variation of mode numbers

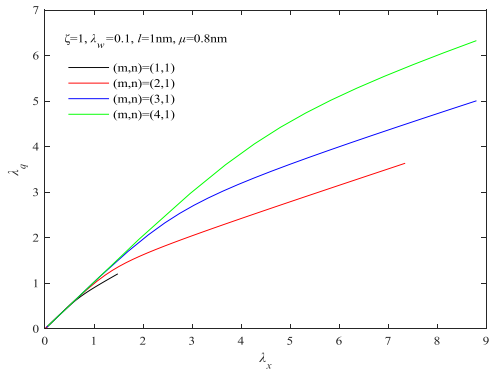

Fig. 15 Dimensionless post-buckling load–shortening curves of imperfect GSs with the variation of mode numbers

curves of imperfect GSs and the comparison of size-dependent dimensionless post-buckling load-shortening curves of imperfect GSs in the theoretical framework of nonlocal strain gradient elasticity theory. From these curves, it is obviously observed that the results predicted by the nonlocal strain gradient theory are lower than those predicted by the classical theory when $\mu > l$; the results predicted by the nonlocal strain gradient theory tend to higher than those predicted by the classical theory when $\mu < l$; the results computed by the nonlcoal strain gradient theory are identical with those computed by the classical theory when $\mu = l$. The reason is that the nonlocal effect that makes the imperfect GSs exert a stiffness-softening effect is slightly dominant than the microstructure effect that makes the imperfect GSs exert a stiffness-enhancement effect at $\mu > l$; But the microstructure effect is larger than the nonlocal effect at $\mu < l$, so that the effective stiffness of the imperfect GSs can be improved significantly; As for $\mu = l$, the double kinds of the size-dependent effect cancel each other out, actually.

Figs. 14 and 15 separately present the dimensionless post-buckling load–deflection curves and load-shortening curves of imperfect GSs with the variation of mode numbers. It can be seen that the increase of the wave mode numbers can remarkably improve the dimensionless post-buckling load-deflection and the dimensionless post-buckling load-shortening of imperfect GSs, indicating that the size-dependent effect is associated with the variation of wave mode numbers. From the viewpoint of physics, that is because the interaction among atoms increases in solids, and thus showing a prominent uptrend for the size-dependent effect at a higher wave model number.

4. Conclusions

The authors in this paper investigate the nonlinear axial-buckling and post-buckling of geometrically imperfect single-layer graphene sheets in the framework of the nonlocal strain gradient theory. Subsequently, with the aid of a two-step perturbation method, a new analytical solution that includes the maximum dimensionless deflection to the sixth power is the first to derive historically, and then a detailed parametric study is performed based on the obtained analytical solution. Finally, several important conclusions are listed as

- What the results of the study is indicating is that there is no significant difference between the solutions to the sixth power and the solutions to the forth power in predicting the responses of a single-layer graphene sheet.
- The initial geometric imperfection plays a significant role in predicting the response of structural components subjected to loading conditions.
- The mechanical performances of nanostructures predicted by the nonlocal strain gradient theory may be smaller than, larger than or equal to those predicted by the classical elasticity theory, depending on the nonlocal parameter, the strain gradient parameter and the ratio of the two scale parameters.
- The size-dependent effect is associated with the variation of wave mode numbers.

Acknowledgments

The authors acknowledge the support from the Hunan Provincial Innovation Foundation for Postgraduate.

(CX20190258).

References

Allahyari, E. and Kiani, A. (2018), "Employing an analytical approach to study the thermo-mechanical vibration of a defective size-dependent graphene nanosheet", *Eur. Phys. J. Plus.*, **133**(6), 223. https://doi.org/10.1140/epjp/i2018-12058-2

Apuzzo, A., Barretta, R., Faghidian, S.A., Luciano, R. and de Sciarra, F.M. (2018), "Free vibrations of elastic beams by modified nonlocal strain gradient theory", *Int. J. Eng. Sci.*, **133**, 99-108. https://doi.org/10.1016/j.ijengsci.2018.09.002

Bao, W., Miao, F., Chen, Z., Zhang, H., Jang, W., Dames, C. and Lau, C.N. (2009), "Controlled ripple texturing of suspended graphene and ultrathin graphite membranes", *Nature Nanotechnol.*, **4**, 562-566. https://doi.org/10.1038/nnano.2009.191

Barati, M.R. (2017), "A general nonlocal stress-strain gradient theory for forced vibration analysis of heterogeneous nanoporous plates", *Eur. J. Mech. A-Solid.*, **67**, 215-230. https://doi.org/10.1016/j.euromechsol.2017.09.001

Barati, M.R. and Zenkour, A.M. (2017a), "Post-buckling analysis of refined shear deformable graphene platelet reinforced beams with porosities and geometrical imperfection", *Compos. Struct.*, **181**, 194-202. https://doi.org/10.1016/j.compstruct.2017.08.082

Barati, M.R. and Zenkour, A.M. (2017b), "Investigating post-buckling of geometrically imperfect metal foam nanobeams with symmetric and asymmetric porosity distributions", *Compos. Struct.*, **182**, 91-98. https://doi.org/10.1016/j.compstruct.2017.09.008

Barati, M.R. and Zenkour, A.M. (2018a), "Vibration analysis of functionally graded graphene platelet reinforced cylindrical shells with different porosity distributions", *Mech. Adv. Mater. Struct.*, **26**(18), 1580-1588. https://doi.org/10.1080/15376494.2018.1444235

Barati, M.R. and Zenkour, A.M. (2018b), "Post-buckling analysis of imperfect multi-phase nanocrystalline nanobeams considering nanograins and nanopores surface effects", *Compos. Struct.*, **184**, 497-505. https://doi.org/10.1016/j.compstruct.2017.10.019

Barati, M.R. and Zenkour, A.M. (2018c), "Thermal post-buckling analysis of closed circuit flexoelectric nanobeams with surface effects and geometrical imperfection", *Mech. Adv. Mater. Struct.*, **26**(17), 1482-1490. https://doi.org/10.1080/15376494.2018.1432821

Barati, M.R. and Zenkour, A.M. (2018d), "Analysis of postbuckling of graded porous GPL-reinforced beams with geometrical imperfection", *Mech. Adv. Mater. Struct.*, **26**(6), 503-511. https://doi.org/10.1080/15376494.2017.1400622

Barati, M.R. and Zenkour, A.M. (2019), "Analysis of postbuckling behavior of general higher-order functionally graded nanoplates with geometrical imperfection considering porosity distributions", *Mech. Adv. Mater. Struct.*, **26**(12), 1081-1088. https://doi.org/10.1080/15376494.2018.1430280

Barretta, R. and Sciarra, F.M.D. (2018), "Constitutive boundary conditions for nonlocal strain gradient elastic nano-beams", *Int. J. Eng. Sci.*, **130**, 187-198. https://doi.org/10.1016/j.ijengsci.2018.05.009

Belkorissat, I., Houari, M.S.A., Tounsi, A., Bedia, E.A. and Mahmoud, S.R. (2015), "On vibration properties of functionally graded nano-plate using a new nonlocal refined four variable mode", *Steel Compos. Struct., Int. J.*, **18**(4), 1063-1081. https://doi.org/10.12989/scs.2015.18.4.1063

Christy, P.A., Peter, A.J. and Lee, C.W. (2018), "Density functional theory on 13C NMR chemical shifts of fullerene", *Solid State Commun.*, **283**, 22-26. https://doi.org/10.1016/j.ssc.2018.08.001

Cong, P.H. and Duc, N.D. (2018), "New approach to investigate the nonlinear dynamic response and vibration of a functionally graded multilayer graphene nanocomposite plate on a viscoelastic Pasternak medium in a thermal environment", *Acta Mech.*, **229**(9), 3651-3670. https://doi.org/10.1007/s00707-018-2178-3

Ebrahimi, F. and Barati, M.R. (2016), "Vibration analysis of piezoelectrically actuated curved nanosize fg beams via a nonlocal strain-electric field gradient theory", *Mech. Adv. Mater. Struct.*, **25**(4), 350-359. https://doi.org/10.1080/15376494.2016.1255830

Ebrahimi, F. and Barati, M.R. (2017), "Hygrothermal effects on vibration characteristics of viscoelastic fg nanobeams based on nonlocal strain gradient theory", *Compos. Struct.*, **159**, 433-444. https://doi.org/10.1016/j.compstruct.2016.09.092

Ebrahimi, F. and Barati, M.R. (2018a), "Damping vibration analysis of graphene sheets on viscoelastic medium incorporating hygro-thermal effects employing nonlocal strain gradient theory", *Compos. Struct.*, **185**, 241-253. https://doi.org/10.1016/j.compstruct.2017.10.021

Ebrahimi, F. and Barati, M.R. (2018b), "Vibration analysis of biaxially compressed double-layered graphene sheets based on nonlocal strain gradient theory", *Mech. Adv. Mater. Struct.*, **26**(10), 854-865. https://doi.org/10.1080/15376494.2018.1430267

Ebrahimi, F., Barati, M.R. and Dabbagh, A. (2016), "A nonlocal strain gradient theory for wave propagation analysis in temperature-dependent inhomogeneous nanoplates", *Int. J. Eng. Sci.*, **107**, 169-182. https://doi.org/10.1016/j.ijengsci.2016.07.008

Faleh, N.M., Ahmed, R.A. and Fenjan, R.M. (2018), "On vibrations of porous FG nanoshells", *Int. J. Eng. Sci.*, **133**, 1-14. https://doi.org/10.1016/j.ijengsci.2018.08.007

Farokhi, H. and Ghayesh, M.H. (2015), "Nonlinear dynamical behaviour of geometrically imperfect microplates based on modified couple stress theory", *Int. J. Mech. Sci.*, **90**, 133-144. https://doi.org/10.1016/j.ijmecsci.2014.11.002

Farokhi, H. and Ghayesh, M.H. (2017), "Nonlinear resonant response of imperfect extensible Timoshenko microbeams", *Int. J. Mech. Mater. Des.*, **13**(1), 43-55. https://doi.org/10.1007/s10999-015-9316-z

Farokhi, H. and Ghayesh, M.H. (2018a), "Supercritical nonlinear parametric dynamics of Timoshenko microbeams", *Commun. Nonlinear Sci.*, **59**, 592-605. https://doi.org/10.1016/j.cnsns.2017.11.033

Farokhi, H. and Ghayesh, M.H. (2018b), "Nonlinear mechanics of electrically actuated microplates", *Int. J. Eng. Sci.*, **123**, 197-213. https://doi.org/10.1016/j.ijengsci.2017.08.017

Farokhi, H., Ghayesh, M.H. and Amabili, M. (2013), "Nonlinear resonant behavior of microbeams over the buckled state", *Appl. Phys. A.*, **113**, 297-307. https://doi.org/10.1007/s00339-013-7894-x

Farokhi, H., Ghayesh, M.H. and Hussain, S. (2016), "Large-amplitude dynamical behaviour of microcantilevers", *Int. J. Eng. Sci.*, **106**, 29-41. https://doi.org/10.1016/j.ijengsci.2016.03.002

Fasolino, A., Los, J.H. and Katsnelson, M.I. (2007), "Intrinsic ripples in graphene", *Nature Mater.*, **6**, 858-861. https://doi.org/10.1038/nmat2011

Ghavanloo, E. (2017), "Axisymmetric deformation of geometrically imperfect circular graphene sheets", *Acta Mech.*, **228**(9), 3297-3305. https://doi.org/10.1007/s00707-017-1891-7

Ghayesh, M.H. (2013), "Subharmonic dynamics of an axially accelerating beam", *Arch App. Mech.*, **82**(9), 1169-1181. https://doi.org/10.1007/s00419-012-0609-5

Ghayesh, M.H. (2018a), "Dynamics of functionally graded

viscoelastic microbeams", *Int. J. Eng. Sci.*, **124**, 115-131. https://doi.org/10.1016/j.ijengsci.2017.11.004

Ghayesh, M.H. (2018b), "Functionally graded microbeams: Simultaneous presence of imperfection and viscoelasticity", *Int. J. Mech. Sci.*, **140**, 339-350. https://doi.org/10.1016/j.ijmecsci.2018.02.037

Ghayesh, M.H. (2018c), "Nonlinear vibration analysis of axially functionally graded shear-deformable tapered beams", *Appl. Math. Model.*, **59**, 583-596. https://doi.org/10.1016/j.apm.2018.02.017

Ghayesh, M.H. (2019a), "Viscoelastic dynamics of axially FG microbeams", *Int. J. Eng. Sci.*, **135**, 75-85. https://doi.org/10.1016/j.ijengsci.2018.10.005

Ghayesh, M.H. (2019b), "Viscoelastic mechanics of Timoshenko functionally graded imperfect microbeams", *Compos. Struct.*, **225**, 110974. https://doi.org/10.1016/j.compstruct.2019.110974

Ghayesh, M.H. (2019c), "Mechanics of viscoelastic functionally graded microcantilevers", *Eur. J. Mech. A/Solid.*, **73**, 492-499. https://doi.org/10.1016/j.euromechsol.2018.09.001

Ghayesh, M.H. (2019d), "Asymmetric viscoelastic nonlinear vibrations of imperfect AFG beams", *Appl. Acoust.*, **154**, 121-128. https://doi.org/10.1016/j.apacoust.2019.03.022

Ghayesh, M.H. (2019e), "Nonlinear oscillations of FG cantilevers", *Appl. Acoust.*, **145**, 393-398. https://doi.org/10.1016/j.apacoust.2018.08.014

Ghayesh, M.H. (2019f), "Resonant vibrations of FG viscoelastic imperfect Timoshenko beams", *J. Vib. Control*, **25**(12), 1823-1832. https://doi.org/10.1177/1077546318825167

Ghayesh, M.H. (2019g), "Viscoelastic nonlinear dynamic behaviour of Timoshenko FG beams", *Eur. Phys. J. Plus*, **134**, 401. https://doi.org/10.1140/epjp/i2019-12472-x

Ghayesh, M.H. and Farokhi, H. (2015), "Chaotic motion of a parametrically excited microbeam", *Int. J. Eng. Sci.*, **96**, 34-45. https://doi.org/10.1016/j.ijengsci.2015.07.004

Ghayesh, M.H. and Moradian, N. (2011), "Nonlinear dynamic response of axially moving, stretched viscoelastic strings", *Arch. Appl. Mech.*, **81**, 781-799. https://doi.org/10.1007/s00419-010-0446-3

Ghayesh, M.H., Yourdkhani, M., Balar, S. and Reid, T. (2010), "Vibrations and stability of axially traveling laminated beams", *Appl. Math. Compos.*, **217**(2), 545-556. https://doi.org/10.1016/j.amc.2010.05.088

Ghayesh, M.H., Kazemirad, S. and Darabi, M.A. (2011), "A general solution procedure for vibrations of systems with cubic nonlinearities and nonlinear/time-dependent internal boundary conditions", *J. Sound Vib.*, **330**(22), 5382-5400. https://doi.org/10.1016/j.jsv.2011.06.001

Ghayesh, M.H., Kazemirad, S. and Reid, T. (2012), "Nonlinear vibrations and stability of parametrically exited systems with cubic nonlinearities and internal boundary conditions: A general solution procedure", *Appl. Math. Model.*, **36**(7), 3299-3311. https://doi.org/10.1016/j.apm.2011.09.084

Ghayesh, M.H., Amabili, M. and Farokhi, H. (2013a), "Coupled global dynamics of an axially moving viscoelastic beam", *Int. J. Non-linear Mech.*, **51**, 54-74. https://doi.org/10.1016/j.ijnonlinmec.2012.12.008

Ghayesh, M.H., Amabili, M. and Farokhi, H. (2013b), "Three-dimensional nonlinear size-dependent behaviour of Timoshenko microbeams", *Int. J. Eng. Sci.*, **71**, 1-14. https://doi.org/10.1016/j.ijengsci.2013.04.003

Ghayesh, M.H., Farokhi, H. and Alici, G. (2016), "Size-dependent performance of microgyroscopes", *Int. J. Eng. Sci.*, **100**, 99-111. https://doi.org/10.1016/j.ijengsci.2015.11.003

Ghayesh, M.H., Farokhi, H. and Gholipour, A. (2017), "Vibration analysis of geometrically imperfect three-layered shear-deformable microbeams", *Int. J. Mech. Sci.*, **122**, 370-383. https://doi.org/10.1016/j.ijmecsci.2017.01.001

Gholipour, A., Farokhi, H. and Ghayesh, M.H. (2015), "In-plane and out-of-plane nonlinear size-dependent dynamics of microplates", *Nonlinear Dyn.*, **79**, 1771-1785. https://doi.org/10.1007/s11071-014-1773-7

Guo, H., Cao, S., Yang, T. and Chen, Y. (2018), "Vibration of laminated composite quadrilateral plates reinforced with graphene nanoplatelets using the element-free IMLS-Ritz method", *Int. J. Mech. Sci.*, **142**, 610-621. https://doi.org/10.1016/j.ijmecsci.2018.05.029

Hashemi, S.H. and Samaei, A.T. (2011), "Buckling analysis of micro/nanoscale plates via nonlocal elasticity theory", *Physica E*, **43**(7), 1400-1404. https://doi.org/10.1016/j.physe.2011.03.012

Hosseini, S.M. and Zhang, C. (2018), "Elastodynamic and wave propagation analysis in a FG graphene platelets-reinforced nanocomposite cylinder using a modified nonlinear micromechanical model", *Steel Compos. Struct., Int. J.*, **27**(3), 255-271. https://doi.org/10.12989/scs.2018.27.3.255

Hosseini, M., Gorgani, H.H., Shishesaz, M. and Hadi, A. (2017), "Size-dependent stress analysis of single-wall carbon nanotube based on strain gradient theory", *Int. J. App. Mech.*, **9**(6), 1750087. https://doi.org/10.1142/S1758825117500879

Hussein, A. and Kim, B. (2018), "Graphene/polymer nanocomposites: The active role of the matrix in stiffening mechanics", *Compos. Struct.*, **202**, 170-181. https://doi.org/10.1016/j.compstruct.2018.01.023

Karami, B., Janghorban, M. and Li, L. (2018), "On guided wave propagation in fully clamped porous functionally graded nanoplates", *Acta Astronaut.*, **143**, 380-390. https://doi.org/10.1016/j.actaastro.2017.12.011

Kazemirad, S., Ghayesh, M.H. and Amabili, M. (2012), "Thermo-mechanical nonlinear dynamics of a buckled axially moving beam", *Arch App. Mech.*, **83**(1), 25-42. https://doi.org/10.1007/s00419-012-0630-8

Kiani, Y. (2017), "Isogeometric large amplitude free vibration of graphene reinforced laminated plates in thermal environment using NURBS formulation", *Comput. Method. Appl. M.*, **332**, 86-101. https://doi.org/10.1016/j.cma.2017.12.015

Korobeynikov, S.N., Alyokhin, V.V. and Babichev, A.V. (2018), "On the molecular mechanics of single layer graphene sheets", *Int. J. Eng. Sci.*, **133**, 109-131. https://doi.org/10.1016/j.ijengsci.2018.09.001

Kumar, D. and Srivastava, A. (2016), "Elastic properties of CNT- and graphene-reinforced nanocomposites using RVE", *Steel Compos. Struct., Int. J.*, **21**(5), 1085-1103. https://doi.org/10.12989/scs.2016.21.5.1085

Li, L., Tang, H. and Hu, Y. (2018), "The effect of thickness on the mechanics of nanobeams", *Int. J. Eng. Sci.*, **123**, 81-91. https://doi.org/10.1016/j.ijengsci.2017.11.021

Lim, C.W., Zhang, G. and Reddy, J.N. (2015), "A higher-order nonlocal elasticity and strain gradient theory and its applications in wave propagation", *J. Mech. Phys. Solids*, **78**, 298-313. https://doi.org/10.1016/j.jmps.2015.02.001

Liu, H., Lv, Z. and Wu, H. (2018), "Nonlinear free vibration of geometrically imperfect functionally graded sandwich nanobeams based on nonlocal strain gradient theory", *Compos. Struct.*, **214**, 47-61. https://doi.org/10.1016/j.compstruct.2019.01.090

Lu, L., Guo, X. and Zhao, J. (2017a), "A unified nonlocal strain gradient model for nanobeams and the importance of higher order terms", *Int. J. Eng. Sci.*, **119**, 265-277. https://doi.org/10.1016/j.ijengsci.2017.06.024

Lu, L., Guo, X. and Zhao, J. (2017b), "Size-dependent vibration analysis of nanobeams based on the nonlocal strain gradient theory", *Int. J. Eng. Sci.*, **116**, 12-24. https://doi.org/10.1016/j.ijengsci.2017.03.006

Ma, H.M., Gao, X.L. and Reddy, J.N. (2008), "A microstructure-

dependent Timoshenko beam model based on a modified couple stress theory", *J. Mech. Phys. Solid.*, **56**(12), 3379-3391. https://doi.org/10.1016/j.jmps.2008.09.007

Malikan, M. and Nguyen, V.B. (2018), "Buckling analysis of piezo-magnetoelectric nanoplates in hygrothermal environment based on a novel one variable plate theory combining with higher-order nonlocal strain gradient theory", *Physica E.*, **102**, 8-28. https://doi.org/10.1016/j.physe.2018.04.018

Malikan, M., Nguyen, V.B. and Tornabene, F. (2018), "Electromagnetic forced vibrations of composite nanoplates using nonlocal strain gradient theory", *Mater. Res. Express*, **5**(7), 075031. https://doi.org/10.1088/2053-1591/aad144

Mcfarland, A.W. and Colton, J.S. (2005), "Role of material microstructure in plate stiffness with relevance to microcantilever sensors", *J. Micromech. Microeng.*, **15**(5), 1060-1067. https://doi.org/10.1088/0960-1317/15/5/024

Meyer, J.C., Geim, A.K., Katsnelson, M.I., Novoselov, K.S., Booth, T.J. and Roth, S. (2007), "The structure of suspended graphene sheets", *Nature*, **446**, 60-63. https://doi.org/10.1038/nature05545

Mirjavadi, S.S., Forsat, M., Barati, M.R., Abdella, G.M., Hamouda, A.M.S., Afshari, B.M. and Rabby, S. (2018a), "Post-buckling analysis of piezo-magnetic nanobeams with geometrical imperfection and different piezoelectric contents", *Microsyst. Technol.*, **25**(9), 3477-3488. https://doi.org/10.1007/s00542-018-4241-3

Mirjavadi, S.S., Afshari, B.M., Barati, M.R. and Hamouda, A.M.S. (2018b), "Transient response of porous fg nanoplates subjected to various pulse loads based on nonlocal stress-strain gradient theory", *Eur. J. Mech. A-Solid.*, **74**, 210-220. https://doi.org/10.1016/j.euromechsol.2018.11.004

Mirjavadi, S.S., Forsat, M., Hamouda, A.M.S. and Barati, M.R. (2019), "Dynamic response of functionally graded graphene nanoplatelet reinforced shells with porosity distributions under transverse dynamic loads", *Mater. Res. Express*, **6**(7), 075045. https://doi.org/10.1088/2053-1591/ab1552

Nematollahi, M.S. and Mohammadi, H. (2019), "Geometrically nonlinear vibration analysis of sandwich nanoplates based on higher-order nonlocal strain gradient theory", *Int. J. Mech. Sci.*, **156**, 31-45. https://doi.org/10.1016/j.ijmecsci.2019.03.022

Novoselov, K.S., Geim, A.K., Morozov, S.V., Jiang, D., Zhang, Y., Dubonos, S.V., Grigorieva, I.V. and Firsov, A.A. (2004), "Electric field effect in atomically thin carbon films", *Science*, **306**(5696), 666-669. https://doi.org/10.1126/science.1102896

Pradhan, S.C. (2009), "Buckling of single layer graphene sheet based on nonlocal elasticity and higher order shear deformation theory", *Phys. Lett. A*, **373**(45), 4182-4188. https://doi.org/10.1016/j.physleta.2009.09.021

Pradhan, S.C. and Murmu, T. (2009), "Small scale effect on the buckling of single-layered graphene sheets under biaxial compression via nonlocal continuum mechanics", *Compos. Mater. Sci.*, **47**(1), 268-274. https://doi.org/10.1016/j.commatsci.2009.08.001

Sadeghirad, A., Su, N. and Liu, F. (2015), "Mechanical modeling of graphene using the three-layer-mesh bridging domain method", *Comput. Method. Appl. Mech. Eng.*, **294**, 278-298. https://doi.org/10.1016/j.cma.2015.06.001

Sahmani, S. and Aghdam, M.M. (2017a), "Nonlinear instability of hydrostatic pressurized hybrid FGM exponential shear deformable nanoshells based on nonlocal continuum elasticity", *Compos. Part B: Eng.*, **114**, 404-417. https://doi.org/10.1016/j.compositesb.2017.01.038

Sahmani, S. and Aghdam, M.M. (2017b), "Nonlocal strain gradient shell model for axial buckling and postbuckling analysis of magneto-electro-elastic composite nanoshells", *Compos. Part B Eng.*, **132**, 258-274. https://doi.org/10.1016/j.compositesb.2017.09.004

Sahmani, S., Bahrami, M. and Aghdam, M.M. (2015), "Surface stress effects on the postbuckling behavior of geometrically imperfect cylindrical nanoshells subjected to combined axial and radial compressions", *Int. J. Mech. Sci.*, **100**, 1-22. https://doi.org/10.1016/j.ijmecsci.2015.06.004

Sahmani, S., Bahrami, M. and Aghdam, M.M. (2016), "Surface stress effects on the nonlinear postbuckling characteristics of geometrically imperfect cylindrical nanoshells subjected to axial compression", *Int. J. Eng. Sci.*, **99**, 92-106. https://doi.org/10.1016/j.ijengsci.2015.10.010

Shafiei, N. and She, G.L. (2018), "On vibration of functionally graded nano-tubes in the thermal environment", *Int. J. Eng. Sci.*, **133**, 84-98. https://doi.org/10.1016/j.ijengsci.2018.08.004

Shahsavari, D., Karami, B. and Mansouri, S. (2017), "Shear buckling of single layer graphene sheets in hygrothermal environment resting on elastic foundation based on different nonlocal strain gradient theories", *Eur. J. Mech. A-Solid.*, **67**(C), 200-214. https://doi.org/10.1016/j.euromechsol.2017.09.004

Shahsavari, D., Karami, B., Fahham, H.R. and Li, L. (2018), "On the shear buckling of porous nanoplates using a new size-dependent quasi-3d shear deformation theory", *Acta Mech.*, 229(11), 4549-4573. https://doi.org/10.1007/s00707-018-2247-7

She, G.L., Yuan, F.G. and Ren, Y.R. (2017a), "Nonlinear analysis of bending, thermal buckling and post-buckling for functionally graded tubes by using a refined beam theory", *Compos. Struct.*, **165**, 74-82. https://doi.org/10.1016/j.compstruct.2017.01.013

She, G.L., Yuan, F.G., Ren, Y.R. and Xiao, W.S. (2017b), "On buckling and postbuckling behavior of nanotubes", *Int. J. Eng. Sci.*, **121**, 130-142. https://doi.org/10.1016/j.ijengsci.2017.09.005

She, G.L., Yuan, F.G. and Ren, Y.R. (2017c), "Research on nonlinear bending behaviors of FGM infinite cylindrical shallow shells resting on elastic foundations in thermal environments", *Compos. Struct.*, **170**, 111-121. https://doi.org/10.1016/j.compstruct.2017.03.010

She, G.L., Yuan, F.G. and Ren, Y.R. (2017d), "Thermal buckling and post-buckling analysis of functionally graded beams based on a general higher-order shear deformation theory", *Appl. Math. Model.*, **47**, 340-357. https://doi.org/10.1016/j.apm.2017.03.014

She, G.L., Yuan, F.G., Karami, B., Ren, Y.R. and Xiao, W.S. (2019), "On nonlinear bending behavior of FG porous curved nanotubes", *Int. J. Eng. Sci.*, **135**, 58-74. https://doi.org/10.1016/j.ijengsci.2018.11.005

Shen, H.S. (2007), "Thermal postbuckling behavior of shear deformable FGM plates with temperature-dependent properties", *Int. J. Mech. Sci.*, **49**(4), 466-478. https://doi.org/10.1016/j.ijmecsci.2006.09.011

Shen, H.S. (2013), *A two-step perturbation method in nonlinear analysis of beams, plates and shells*, Higher Education Press.

Shen, H.S. and Zhang, J.W. (1988), "Perturbation analyses for the postbuckling of simply supported rectangular plates under uniaxial compression", *App. Math. Mech.*, **9**(8), 793-804. https://doi.org/10.1007/BF02465403

Shen, H.S., Xiang, Y., Lin, F. and Hui, D. (2017), "Buckling and postbuckling of functionally graded graphene-reinforced composite laminated plates in thermal environments", *Compos. Part B Eng.*, **119**, 67-78. https://doi.org/10.1016/j.compositesb.2017.03.020

Shen, H.S., Xiang, Y., Fan, Y. and Hui, D. (2018), "Nonlinear bending analysis of FG-GRC laminated cylindrical panels on elastic foundations in thermal environments", *Compos. Part B: Eng.*, **15**, 148-157. https://doi.org/10.1016/j.compositesb.2017.12.048

Singh, S. and Patel, B.P. (2018), "A computationally efficient multiscale finite element formulation for dynamic and

postbuckling analyses of carbon nanotubes", *Comput. Struct.*, **195**, 126-144. https://doi.org/10.1016/j.compstruc.2017.10.003

Soleimani, A., Dastani, K., Hadi, A. and Naei, M.H. (2019), "Effect of out-of-plane defects on the postbuckling behavior of graphene sheets based on nonlocal elasticity theory", *Steel Compos. Struct., Int. J.*, **30**(6), 517-534. https://doi.org/10.12989/scs.2019.30.6.517

Tahouneh, V., Naei, M.H. and Mashhadi, M.M. (2018), "The effects of temperature and vacancy defect on the severity of the SLGS becoming anisotropic", *Steel Compos. Struct., Int. J.*, **29**, 647-657. https://doi.org/10.12989/scs.2018.29.5.647

Wang, Q. (2005), "Wave propagation in carbon nanotubes via nonlocal continuum mechanics", *J. Appl. Phys.*, **98**, 124301. https://doi.org/10.1063/1.2141648

Wang, J., Xie, H. and Guo, Z. (2017), "First-principles investigation on thermal properties and infrared spectra of imperfect graphene", *Appl. Therm. Eng.*, **116**, 456-462. https://doi.org/10.1016/j.applthermaleng.2016.12.087

Wang, Y., Feng, C., Zhao, Z. and Yang, J. (2018), "Eigenvalue buckling of functionally graded cylindrical shells reinforced with graphene platelets (GPL)", *Compos. Struct.*, **202**, 38-46. https://doi.org/10.1016/j.compstruct.2017.10.005

Wu, C.P. and Chen, Y.J. (2018), "Cylindrical Bending Vibration of Multiple Graphene Sheet Systems Embedded in an Elastic Medium", *Int. J. Struct. Stab. Dyn.*, **19**(4), 1950035. https://doi.org/10.1142/S0219455419500354

Wu, X., Mu, F., Wang, Y. and Zhao, H. (2018), "Application of atomic simulation methods on the study of graphene nanostructure fabrication by particle beam irradiation: A review", *Compos. Mater. Sci.*, **149**, 98-106. https://doi.org/10.1016/j.commatsci.2018.03.022

Xu, X.J., Zheng, M.L. and Wang, X.C. (2017), "On vibrations of nonlocal rods: Boundary conditions, exact solutions and their asymptotics", *Int. J. Eng. Sci.*, **119**, 217-231. https://doi.org/10.1016/j.ijengsci.2017.06.025

Yan, J.W. and Lai, S.K. (2018), "Superelasticity and wrinkles controlled by twisting circular graphene", *Comput. Method. Appl. Mech. Eng.*, **338**, 634-656. https://doi.org/10.1016/j.cma.2018.04.049

Yang, J., Wu, H. and Kitipornchai, S. (2016), "Buckling and postbuckling of functionally graded multilayer graphene platelet-reinforced composite beams", *Compos. Struct.*, **161**, 111-118. https://doi.org/10.1016/j.compstruct.2016.11.048

Yang, J., Dong, J. and Kitipornchai, S. (2018a), "Unilateral and bilateral buckling of functionally graded corrugated thin plates reinforced with graphene nanoplatelets", *Compos. Struct.*, **209**, 789-801. https://doi.org/10.1016/j.compstruct.2018.11.025

Yang, Z., Liew, K.M. and Hui, D. (2018b), "Characterizing nonlinear vibration behavior of bilayer graphene thin films", *Compos. Part B Eng.*, **145**, 197-205. https://doi.org/10.1016/j.compositesb.2018.03.004

Yengejeh, S.I., Kazemi, S.A., Ivasenko, O. and Öchsner, A. (2017), "Simulations of Graphene Sheets Based on the Finite Element Method and Density Functional Theory: Comparison of the Geometry Modeling under the Influence of Defects", *J. Nano. Res-sew.*, **47**, 128-135. https://doi.org/10.4028/www.scientific.net/JNanoR.47.128

Zenkour, A.M. and Abouelregal, A.E. (2015), "Thermoelastic interaction in functionally graded nanobeams subjected to time-dependent heat flux", *Steel Compos. Struct., Int. J.*, **18**(4), 909-924. https://doi.org/10.12989/scs.2015.18.4.909

Zhan, H.Z., Yang, F.P. and Wang, X. (2018), "Nonlinear dynamic characteristics of bi-graphene sheets/piezoelectric laminated films considering high order van der Walls force and scale effect", *Appl. Math. Model.*, **56**, 289-303. https://doi.org/10.1016/j.apm.2017.11.038

Zhang, J., Zhang, W., Ragab, T. and Basaran, C. (2018), "Mechanical and electronic properties of graphene nanomesh heterojunctions", *Comp. Mater. Sci.*, **153**, 64-72. https://doi.org/10.1016/j.commatsci.2018.06.026

Zhu, X. and Li, L. (2017), "Closed form solution for a nonlocal strain gradient rod in tension", *Int. J. Eng. Sci.*, **119**, 16-28. https://doi.org/10.1016/j.ijengsci.2017.06.019

CC